

1983

Steel bridge members under variable amplitude, long life fatigue loading, Final report, September 1983,85p.

John W. Fisher

Dennis R. Mertz

An Zhong

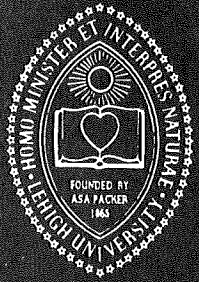
Follow this and additional works at: <http://preserve.lehigh.edu/engr-civil-environmental-fritz-lab-reports>

Recommended Citation

Fisher, John W.; Mertz, Dennis R.; and Zhong, An, "Steel bridge members under variable amplitude, long life fatigue loading, Final report, September 1983,85p." (1983). *Fritz Laboratory Reports*. Paper 517.
<http://preserve.lehigh.edu/engr-civil-environmental-fritz-lab-reports/517>

This Technical Report is brought to you for free and open access by the Civil and Environmental Engineering at Lehigh Preserve. It has been accepted for inclusion in Fritz Laboratory Reports by an authorized administrator of Lehigh Preserve. For more information, please contact preserve@lehigh.edu.

**Lehigh
University**



LEHIGH UNIVERSITY LIBRARIES



3 9151 00942860 4

STEEL BRIDGE MEMBERS UNDER VARIABLE AMPLITUDE, LONG LIFE FATIGUE LOADING

Final Report

by

**John W. Fisher
Dennis R. Mertz
An Zhong**

**Fritz
Engineering
Laboratory**

Report No. 463-1(83)

Acknowledgment

This work was sponsored by the American Association of State Highway and Transportation Officials, in cooperation with the Federal Highway Administration and was conducted in the National Cooperative Highway Research Program which is administered by the Transportation Research Board of the National Research Council.

Disclaimer

This copy is an uncorrected draft as submitted by the research agency. A decision concerning acceptance by the Transportation Research Board and publication in the regular NCHRP series will not be made until a complete technical review has been made and discussed with the researchers. The opinions and conclusions expressed or implied in the report are those of the research agency. They are not necessarily those of the Transportation Research Board, the National Academy of Sciences, the Federal Highway Administration, the American Association of State Highway and Transportation Officials, or of the individual states participating in the National Cooperative Highway Research Program.

TABLE OF CONTENTS

	<u>Page</u>
ACKNOWLEDGMENTS	v
SUMMARY	vi
1. INTRODUCTION AND RESEARCH APPROACH	1
Background	1
Objectives and Scope	3
Research Approach	4
Full-Scale As-Welded Beam Tests	4
Fatigue Crack Growth Tests	9
Random Block Loading of Cruciform Specimens	11
2. FINDINGS	14
Fatigue Behavior of Web Attachments	14
Fatigue Behavior of Cover Plates	15
Fatigue Crack Growth Under Random Variable Loading	17
Fatigue Behavior of Nonload-Carrying Welds Under Random Variable Block Loading	17
3. RESULTS AND EVALUATION OF EXPERIMENTAL DATA	19
Fatigue Behavior of Welded Web Attachments	20
Fatigue Behavior of Welded Cover Plates	22
Fatigue Crack Growth Under Random Variable Loading	24
Fatigue Behavior of Nonload-Carrying Welds Under Random Variable Block Loading	27
4. CONCLUSIONS AND APPLICATION OF RESULTS	29
5. RECOMMENDATIONS FOR FURTHER RESEARCH	32

	<u>Page</u>
TABLES	35
FIGURES	37
APPENDIX	75
REFERENCES	83

ACKNOWLEDGMENTS

The research reported herein was performed under NCHRP Project 12-15(4) by the Fritz Engineering Laboratory, Lehigh University, with John W. Fisher, Professor of Civil Engineering, as principal investigator. The other authors of this report are Dennis R. Mertz, Research Assistant, and An Zhong, Visiting Research Engineer.

Special thanks are extended to Fritz Laboratory staff members Richard Sopko, who was responsible for photographic coverage, and John M. Gera and Sharon Balogh, who were responsible for drafting the illustrations. Robert Dales and Charles Hittinger, laboratory foremen, and their staff provided valuable assistance during the test setup and actual testing. Sincere thanks are also due Ruth Grimes, who provided assistance and typed the final manuscript and many reports during the course of the project. The authors are also indebted to Research Assistants: Bruce Ward, James Bellenoit, Sainath Venkatachalam, Deborah Marcotte, Antonello DeLuca, William Frank, John Nedley, Peter Keating, and Johannes Out, who provided daily inspection of the test beams.

Thanks are also due Hugh T. Sutherland for developing the random control devices and storage units that were used to program the random variable tests on the dynamic tests and in the Amsler Vibrophore.

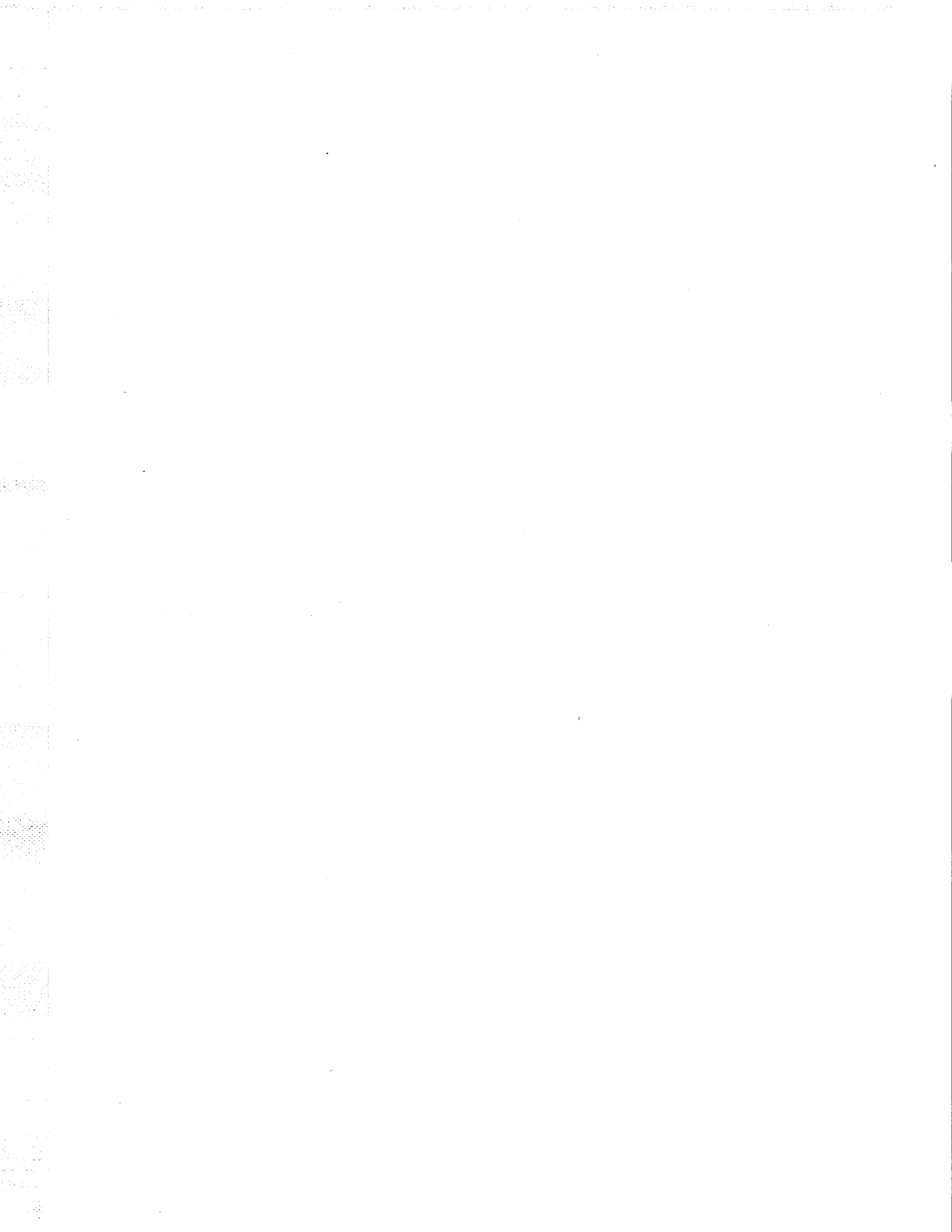
SUMMARY

The research described in this report is the result of studies performed under NCHRP Project 12-15(4). It is intended to provide information on evaluating the fatigue resistance of welded attachments subjected to variable amplitude fatigue loading. The main portion of the research consisted of laboratory studies of welded attachments under random variable amplitude load spectra defined by a Rayleigh-type distribution with most stress-cycles below the constant amplitude fatigue limit. (Some stress cycles exceeded this limit.) Eight full-size beams with web attachments and cover plates were tested during the program.

Fatigue crack growth data was generated utilizing random block variable amplitude stress spectra defined by a Rayleigh-type distribution. The intent was to extend the existing data into the region below the constant amplitude crack growth threshold. Also, nonload-carrying fillet welded cruciform-type specimens were tested under simple bending using a random variable amplitude block loading to supplement the existing shorter life studies carried out on stiffener details.

The results obtained from these variable amplitude tests are consistent with the previously reported constant amplitude test. However, the existence of a fatigue limit below which no fatigue cracks propagate is assured only if none of the stress range cycles exceed this constant amplitude fatigue limit. If any of the stress range cycles (as few as one per thousand cycles) exceed the limit, fatigue crack propagation will likely occur.

The random variable test data from the beam specimens generally fell between the upper and lower confidence limits projected from constant cycle data. The smaller simulated details generally resulted in the random variable test data falling near the upper confidence limit of constant amplitude test results.



1. INTRODUCTION AND RESEARCH APPROACH

BACKGROUND

Existing test data for specimens subjected to random variable amplitude loading with most stress cycles below the constant amplitude fatigue limit (some stress cycles exceeding this limit) is sparse. This region of behavior is illustrated in Fig. 1. Three cover-plated beams reported in NCHRP Report 188 (1) and a few tests on simple tensile specimens with nonload-carrying fillet welds reported by Albrecht (2) indicate that fatigue cracks develop even though the effective stress range is well below the crack growth threshold or fatigue limit.

In NCHRP Study 12-12 about 8% of the variable stress cycles exceeded the constant amplitude fatigue limit. In the University of Maryland study the three specimens tested near the fatigue limit had about 2.8% of the stress cycles exceeding the constant amplitude fatigue limit for Category C. Other specimens exceeded this limit by 15.6% to 100%.

The cover-plated beams at Yellow Mill Pond have developed cracking at a large number of cover plate ends (3). These cracks have developed in beams which were only infrequently subjected to stress ranges that exceeded the constant amplitude fatigue limit of the Category E'. For example, small cracks were detected in several beams where only 0.1% of the measured stress cycles exceeded the estimated fatigue limit for Category E'. Hence, observed field behavior suggests that the conditions at Category E and E' details may become more serious if increased loads use bridge structures in the future. The consequences of occasional overloads from permits and other sources may be more critical than previously assumed.

Tilly and Nunn have investigated the low stress fatigue behavior of small scale welded steel joints subjected to random variable amplitude loading (4). The percentage of cycles exceeding the constant amplitude fatigue limit varied from 0.24% to 85.0%. Figure 2 shows the two classes (Classes F and G in the British Standard for Bridge Design; Category E in the AASHTO Specification) of specimens tested. Two types of stress spectra were utilized to simulate random variable amplitude loads. These are shown in Fig. 3. The Class F connections have nonload-carrying fillet welded attachments on the plate surfaces and were subjected to the Rayleigh spectrum and the axle spectrum. The Class G connections were axial specimens having attachments welded to their edges. These specimens were subjected to the axle spectrum only in order to ascertain the effect of spectrum versus joint type on the behavior. The conclusions drawn from the tests subjected to the Rayleigh spectra were that if the stresses below the constant amplitude fatigue limit are ignored, calculated fatigue lives can be too optimistic. From the axle spectra tests, Tilly and Nunn found that fatigue life was enhanced due to retardation of the crack propagation rate due to extremely small numbers of high stresses.

Additional fatigue tests are needed on details subjected to random variable amplitude loading to determine the consequences of cycles exceeding the constant amplitude fatigue limit. Existing data do not provide an indication of the frequency of occurrence necessary to initiate and sustain fatigue crack growth. The three known test series had between 0.24% and 100% of their stress cycles exceeding the constant amplitude fatigue limit, but little or no replication of data was obtained. For the stiffener

detail which is a Category C detail, the peak stress range in the spectrum was 110 MPa (16 ksi) which was 33% above the constant amplitude fatigue limit of 83 MPa (12 ksi). For the Category E cover-plated beam in which 8% of the stress cycles exceeded 34 MPa (5 ksi), the peak stress range was 41 MPa (6 ksi) or 20% above the constant amplitude fatigue limit.

OBJECTIVES AND SCOPE

The objective of this study is to expand the current knowledge of the behavior of welded bridge details subjected to variable-amplitude loading with a relatively small frequency of occurrence of stress cycles above the constant amplitude fatigue limit. To accomplish this, full-scale beams were tested with welded cover plates and web attachments to see how these results compare to smaller scale test specimens. Additional small scale specimens were also tested to expand this available data base.

To fulfill these objectives the following three tasks were established:

1. To evaluate the fatigue strength of beams with web and flange Category E or E' attachment details and to investigate the adequacy of drilling holes as a retrofit technique to arrest crack growth and prevent further cracking.
2. To extend the variable amplitude crack growth data and effective stress intensity range developed by Barsom and Novak (5) into the region below the constant amplitude crack growth threshold. Basic fatigue crack growth specimens tested under random variable amplitude block loading were to be used for this study.

3. To supplement the shorter life studies carried out by Albrecht (2) on a stiffener (Category C) detail by testing nonload-carrying fillet welded cruciform type specimens under simple bending using a random variable amplitude block loading. These tests would provide longer life data.

RESEARCH APPROACH

Full-Scale As-Welded Beam Tests

Because welded details have complex initial discontinuities and variable stress concentration conditions, the primary study was carried out on rolled beam sections with as-welded details as opposed to small scale test specimens. Two basic parameters were examined for the random variable stress spectrum. One was the frequency of occurrence of stress cycles above the constant amplitude fatigue limit. The second condition is the magnitude of the peak stress range in the stress spectrum. In order to provide adequate levels of replication for the test details, three web gussets were attached to the test beams in the constant moment region. Cover plates were attached to the flanges in the shear spans. The stress range at the end of the cover plates was made equal to about 95% of the stress range at the ends of the web gusset plates. Hence, each test beam provided eight distinct weld ends for crack development as illustrated in Fig. 4.

The eight full-size as-welded beams tested during the course of this project were rolled W18X50 beams of A588 steel. The welded attachments were fabricated from A36 steel.

The beams were 4.9 m (16 ft.) long and tested on a 4.6 m (15 ft.) span under four-point loading, as shown in Fig. 4. Each beam had three 25.4 mm (1 in.) thick, 102 mm (4 in.) wide, 305 mm (12 in.) long gusset plates fillet welded in the 1.5 m (5 ft.) constant moment region (see Fig. 5). Some of the 16 mm (5/8 in.) fillet welds wrapped completely around the gusset plates, while others consisted of longitudinal welds alone. The beams also had 25.4 mm (1 in.) thick cover plates welded to each flange located in the two shear spans, so as to have approximately 95% of the stress at the web details at the coverplate ends. Some of the cover plates had transverse end welds and longitudinal fillet welds, while others were attached with longitudinal fillet welds alone.

Coupon tension specimens taken from the girder flanges (ASTM - A370) gave an average yield point of 449 MPa (65.1 ksi). The average ultimate tensile strength was 537 MPa (77.9 ksi). The average elongation of the specimens was 22.2%.

A wide band Rayleigh-type stress spectrum was utilized for this test program. This type of distribution is shown in Fig. 6. The control variables for the experiment were:

1. the effective stress range, $S_{rRMC} = \left[\sum \alpha_i S_{ri}^3 \right]^{1/3}$, and
2. the frequency of exceedance of the constant amplitude fatigue limit, $\Sigma \gamma_{if}$.

The values of S_{rRMC} , are shown in Table 1 for each test beam. Seven different exceedances were investigated for the web and flange details ranging from 0.0 to 10.16%. As shown in Table 1, the width of the Rayleigh

distribution, W (see Fig. 6) used for the four pairs of tests was 3.75, 4.0, 4.75, and 4.75, respectively.

All beams were fabricated by a bridge fabrication shop in the Bethlehem, Pennsylvania area. The fabricator was instructed to use normal fabrication and inspection procedures. All rolled sections were produced from the same heat.

All beams were tested on the dynamic test bed in the Fritz Engineering Laboratory at Lehigh University (see Fig. 7). Two beams were tested simultaneously in order to maximize the test data acquired over the relatively long period required to complete each test. This configuration is shown in Fig. 8.

The variable amplitude cyclical load was applied with an MTS system consisting of two hydraulic jacks each with a capacity of 890 kN (195 kips). Each loading cycle was nearly sinusoidal; the minimum applied stress was always tensile and varied from 6.2 MPa (0.9 ksi) to 16.5 MPa (2.4 ksi). All testing was carried out at room temperatures between 15° C (60° F) and 27° C (80° F).

A wide band Rayleigh-type probability-density curve was utilized to define the stress cycles that were randomly applied to the two test beams. This probability-density curve was defined as follows:

$$P = \frac{P'}{S_{rd}} = \text{probability density} \left(\text{units} = \frac{1}{\text{force per area}} \right) \quad (1)$$

where
$$p' = C x' e^{-\left(\frac{1}{2}\right)(x')^2} \quad (1a)$$

$$S_{rd} = \frac{S_{rmax} - S_{rmin}}{W} \quad (1b)$$

where $C =$ correction factor to account for finite nature of the distribution used

$$x' = \frac{S_r - S_{rmin}}{S_{rd}}$$

$W =$ width of assumed distribution

For the Rayleigh distribution, the effective stress range derived from Miner's Rule is given by

$$S_{rRMC} = \left(\sum \alpha_i S_{ri}^3 \right)^{\frac{1}{3}} \quad (2)$$

The Rayleigh distribution provides a value of S_{rRMC} that is

$$S_{rRMC} = S_{rmin} + 1.5 S_{rd} \quad (3)$$

The root-mean-cube (RMC) stress range is about 29% greater than the root-mean-square (RMS) stress range for $W = 3.0$.

A typical plot of the stress range, S_r versus probability density (along with some of the above defined variables) is shown in Fig. 6. Also shown in Fig. 6 is $\Sigma \gamma_{if}$ which defines the frequency of occurrence of stress cycles above the constant amplitude fatigue limit.

The simulated variable amplitude load was applied as a large block of 1024 randomized loads of ten different magnitudes. This large block was approximately five minutes in duration and was continuously repeated. A typical stress spectrum was divided into ten discrete increments of stress range with their magnitude varying from 10 MPa to 41 MPa (1.5 ksi to 6.0 ksi) and their corresponding number of occurrences (totaling 1024) is shown in Fig. 9. The sequence of the 1024 occurrences was developed from a random number generator.

Figure 10 shows a small portion of the random variable stress cycles as a function of time. As is apparent, the larger stress cycles required more time than smaller amplitude stress cycles.

Each beam was cycled until a crack was detected at a detail. Generally, the examination was made visually with 10X magnification. During the course of the study several different crack detection procedures were evaluated in addition to the visual examination. They included, liquid penetrant, ultrasonic shear wave and acoustical emission.

All web details were permitted to develop through-thickness cracks, that were about 25.4 mm (1 in.) long before being retrofitted. The cover-plated flange details on four of the beams were retrofitted after marking the crack front before the crack completely penetrated the flange. Having defined the fatigue life corresponding to the through thickness crack at the detail, an appropriate retrofitting procedure was applied, in order to arrest crack growth and prevent the cross-section from being destroyed. Cracked web attachment details were retrofitted by drilling holes at the tip of the through thickness web cracks. Cracked cover plate ends were

retrofitted by clamping splice plates over the detail. The test was then continued in order to determine the fatigue behavior and life of the other details and to establish the effectiveness of the drilling of holes as a retrofit procedure. This procedure was repeated for each detail as cracking developed, and this permitted the fatigue strengths of all details on a beam to be determined.

Fatigue Crack Growth Tests

Most fatigue crack propagation tests have been carried out under constant amplitude cyclic load fluctuation. Incremental crack lengths and elapsed load cycles are used to determine the crack growth rate da/dN and the corresponding fluctuation of the stress intensity factor ΔK .

Under variable amplitude random sequence loading, the magnitude of ΔK changes with each load cycle. Barsom has used the root-mean-square stress intensity as a means of defining the crack growth rate under variable amplitude load (5). The root-mean-square of the stress intensity range, ΔK_{RMS} , was estimated for each crack growth increment.

In this study, the root-mean-cube stress intensity factor was used to define the effective stress intensity factor corresponding to the crack growth rate increment. This used the effective stress range provided by Eq. 2 for the cyclic stress range applied during the crack growth increment.

The fatigue crack growth data was obtained by using 6 mm (1/4 in.) thick center crack specimens as illustrated in Figs. 11 and 12. Each specimen had two fatigue cracks, so that data could be acquired from both

in view of the large numbers of stress cycles that were to be applied as a result of the random variable loading.

The specimens were all fabricated from the same A36 steel plate. All specimens were machined to the configuration shown in Fig. 12. The length was 311 mm (12.25 in.), and the width was selected as 89 mm (3.5 in.). A smooth and uniform surface was achieved on each specimen by a milling and grinding process on both faces which reduced the thickness to 6 mm (1/4 in.)

After machining to size, a 3 mm (1/8 in.) hole was drilled in the center of the specimen to facilitate machining the starter notches. The notches were all machined into the specimens with an electrical discharge process.

The specimens were tested under variable amplitude, random block sequence loading at a frequency of about 160 cycles per second. The test setup is shown in Fig. 13.

The fatigue crack growth increments were measured optically using a microscope mounted in a micrometer slide. A mylar tape with .127 mm (.005 in.) subdivision scale was attached to the plate surface along a line parallel to the crack path so that the crack lengths could be monitored at both cracks (see Fig. 14).

The load range spectra frequency of occurrence corresponded to a Rayleigh distribution with $S_{rd}/S_{rm} = 0.5$ and the band width $W = \frac{S_{rmax} - S_{rmin}}{S_{rd}} = 3$, as illustrated in Fig. 15. Eight levels of stress range were selected to approximate the truncated Rayleigh distribution. The eight load levels were randomized into 150 blocks with each block

having 960 cycles of load applied at a constant amplitude within the block. Figure 16 shows the randomized block sequence that was used for the studies.

Three levels of stress ratio defined as:

$$R = \frac{\text{Mean Stress} - S_{rRMC}}{\text{Mean Stress} + S_{rRMC}} \quad (4)$$

were used during the test program. S_{rRMC} is the root mean cube stress range of the variable load spectrum as defined by Eq. 2. The levels of R selected were 0.3, 0.55, and 0.8. The higher ratios correspond to the conditions that exist in welded joints as a result of residual tensile stresses.

The test data acquired was intended to examine the $da/dN - \Delta K$ region at much lower levels than evaluated by Barsom and Novak (5). The test procedures used during the tests followed the recommendations given in Refs. 6 and 7.

Random Block Loading of Cruciform Specimens

The earlier tests by Albrecht were carried out on A588 steel specimens with nonload-carrying fillet welds. Thirteen tests were reported on a tensile specimen 10 mm x 26 mm (3/8 in. x 1 in.) in cross-section to which 6 mm (1/4 in.) thick plates were transverse welded with 6 mm (1/4 in.) fillet welds. The random variable stress range spectrum represented a skewed distribution. The effective root mean cube stress range, S_{rRMC} , varied between 50.5 MPa (7.3 ksi) and 177 MPa (25.7 ksi).

In this study similar cruciform type joints were tested in bending as illustrated in Fig. 17. Both constant load cycle and variable load cycle tests were carried out. The test specimens were fabricated from A514 steel plate and were available from an earlier study carried out by Frank (8). The primary plate cross-section was 16 mm x 30.5 mm (5/8 in. x 1-1/4 in.) and had 16 mm (5/8 in.) thick plates transverse welded to the main plate with 12 mm (1/2 in.) fillet welds. The specimens were all fabricated from a 610 mm x 533 mm (24 in. x 21 in.) plate to which two 16 mm x 50 mm x 610 mm (5/8 in. x 2 in. x 24 in.) plates were submerged arc welded to each side. Three weld passes were made for each 12 mm (1/2 in.) weld in a sequence to minimize distortion. The test specimens were then saw cut from the plate and milled to their final 30.5 mm (1-1/4 in.) width.

The variable load cycle test specimens were all tested using the same variable amplitude random block loading sequence that was used for the crack growth studies. Strain gages were attached to each specimen in order to control and monitor the magnitude of the cyclic stresses. The tests were carried out in the Amsler Vibrophore at a frequency of about 160 cycles per second for both variable and constant cycle loading. Figure 17 shows a specimen and the test setup in the Vibrophore.

The variable load cycle tests were carried out at effective root-mean cube stress ranges of 122 MPa (17.7 ksi), 133 MPa (19.3 ksi), 163 MPa (23.7 ksi), 178 MPa (25.8 ksi), and 207 MPa (30 ksi). The corresponding maximum stress ranges in the variable load spectrum were 196 MPa (28.5 ksi), 215 MPa (31.3 ksi), 263 MPa (38.1 ksi), 286.6 MPa (41.5 ksi), and 333 MPa

(48.3 ksi). The mean stress varied between 212 MPa and 222 MPa (30.7 ksi to 32.2 ksi) and was dependent on the resonant response of individual specimens.

Constant amplitude tests were also carried out at stress ranges of 152 MPa (22 ksi), 166 MPa (24 ksi), 196 MPa (28.4 ksi), 263 MPa (38.1 ksi), and 333 MPa (48.3 ksi).

Because of the high frequency of loading, no effort was made to detect fatigue crack initiation. The fatigue life was defined by failure to maintain resonant loading on the test specimen. This generally corresponded to a crack about halfway through the plate thickness, as illustrated in Fig. 18.

2. FINDINGS

The findings of NCHRP Project 12-15(4) are summarized in this chapter. A detailed evaluation of the experimental data is given in Chapter Three. Documentation of the test results is provided in Appendix A.

FATIGUE BEHAVIOR OF WEB ATTACHMENTS

1. When the effective stress range of the applied stress spectrum was below the constant amplitude fatigue limit, both types of attachments either equaled or exceeded the fatigue resistance provided by an extension of the Category E' line at a slope of approximately three to one on a log-log plot. As long as a portion of the applied stress spectrum was above the constant amplitude fatigue limit (even though the effective stress range was below this limit) fatigue cracking occurred. This situation is graphically illustrated in Fig. 1. The results suggest that all of the stress cycles contributed to the fatigue damage as the scatter in the test data is not much greater than experienced with constant cycle tests.
2. At web attachments where the welds wrapped completely around the gusset plate, the toe of the transverse fillet weld joining the plate to the web provided the fatigue crack initiation sites. At web attachments without such transverse welds, the termination of the longitudinal welds provided initiation sites. Fatigue cracking propagated from these sites, because

of the stress concentration that developed as a result of the geometric conditions and the greater probability of microscopic discontinuities at the fillet weld toe.

3. When the effective stress range was above the constant amplitude fatigue limit, both types of welded web attachments tested either equaled or exceeded the fatigue resistance provided by Category E' of the AASHTO Specifications when plotted as a function of the effective stress range, S_{rRMC} , versus life.

FATIGUE BEHAVIOR OF COVER PLATES

1. When the effective stress range of the applied stress spectrum was below the constant amplitude fatigue limit, similar behavior with regard to straight line extensions of the Category E and E' S-N lines was observed, which was comparable to the web details. Hence, as long as a portion of the stress range spectrum exceeded the constant amplitude fatigue limit, fatigue cracking occurred. At two cover plates where no stress range cycles exceeded the estimated constant amplitude fatigue limit for Category E, the cover plate details were found to have developed very small semielliptical cracks after 100 million cycles when the details were destructively broken open in an attempt to reveal cracking. These single semielliptical cracks were found to be about 1 mm (0.04 in.) deep.

2. At cover plates where the welds wrapped completely around the cover plates, the toe of the transverse fillet weld joining the plate to the flange provided fatigue crack initiation sites. At cover plates without such transverse welds, the termination of the longitudinal welds provided the initiation sites. Crack propagation developed from these sites which are in a region of stress concentration.

3. When the effective stress range was above the constant amplitude fatigue limit, both types of cover plate details either equaled or exceeded the fatigue resistance of Category E' when first observed cracking is used. The additional observed and estimated life corresponding to severing the flange, increased the fatigue life in all but two cases to at least halfway between the straight line extension of Categories E and E' sloped lines. Four details were near this midpoint. The ten remaining details exceeded the lower limit provided by Category E.

4. The results of the extreme life cover plated beam details were found to be comparable to the results reported in NCHRP Report 188 (1) at the higher effective stress range levels (see Fig. 24). The three test results from that study that were acquired at a 21 MPa (3 ksi) effective stress range were also comparable to the extreme life results observed in this study.

FATIGUE CRACK GROWTH UNDER RANDOM VARIABLE LOADING

The test data indicated that the effective stress intensity factor derived from Eq. 2 provided reasonable correlation with the crack growth relationship developed for constant cycle tests when extrapolated into the low levels of crack growth rate. Additional work is needed at very low levels of ΔK_{RMC} .

The variable amplitude crack growth threshold was found to be much lower than the constant cycle crack growth threshold. At the 0.8 R-ratio, the value tended to approach 2.4 MPa \sqrt{m} (2.2 ksi $\sqrt{in.}$) before the crack growth rate approached zero. The test results confirm that the average range of crack growth per cycle, da/dN , under random variable loading can be related to the crack growth relationship derived from constant amplitude tests if the effective stress intensity range is estimated from Eq. 2. This relationship can be extended below the constant cycle crack growth threshold when some of the stress intensity range cycles in the variable amplitude stress spectrum exceeds the constant cycle crack growth threshold.

The root-mean-cube effective stress intensity factor and crack growth behavior appear to be comparable to the behavior of the welded details.

FATIGUE BEHAVIOR OF NONLOAD-CARRYING WELDS

UNDER RANDOM VARIABLE BLOCK LOADING

1. The limited constant cycle amplitude tests of the cruciform type specimens subjected to bending were observed to provide a fatigue resistance that was near the upper bound of other tests on similar type specimens (20,21). The results were analogous to the resistances reported by Albrecht (2), Goerg (20), and Mueller (21).

2. The variable amplitude tests were found to plot near the upper bound of the constant cycle tests. The test results suggested a constant cycle fatigue limit of about 152 MPa (22 ksi). The variable amplitude data relationship to the constant cycle data was somewhat comparable to the observations reported by Tilly and Nunn (4) and Albrecht (2). Hence, all of the smaller simulated specimens tested to date tend to provide longer fatigue lives and higher fatigue resistance when subjected to random variable loading than do the beam type specimens.

3. RESULTS AND EVALUATION OF EXPERIMENTAL DATA

During this experimental study, test data was acquired on welded web attachments and cover-plated beams subjected to random variable loading. The data included the applied stresses as measured by strain gages and correlated by bending theory, cycles at which fatigue cracking was first detected, cycles to failure, and observations on crack growth behavior.

In addition to the beam fatigue tests, test data was also acquired on fatigue crack growth under random block loading. The test specimen used to acquire this information was an axially loaded plate specimen with two through thickness center cracks as illustrated in Fig. 11. This permitted test data to be acquired from both cracks and optimized the data base as extreme numbers of repeated load cycles were applied. The crack growth rates of interest were in the crack growth threshold region when ΔK was less than $5.5 \text{ MPa } \sqrt{\text{m}}$ ($5 \text{ ksi } \sqrt{\text{in.}}$) and the rate of crack growth was less than 10^{-7} mm/cycle (10^{-6} /cycle).

Bending tests are also reported on welded cruciform specimens subjected to random variable block loading comparable to the crack growth specimens and several of the test beams. These loads produced fatigue crack growth at the transverse fillet weld toes of the short attachments that were welded to the plate surface.

Each of these tests are discussed in detail in this chapter.

FATIGUE BEHAVIOR OF WELDED WEB ATTACHMENTS

Prior to conducting this test series, the only known fatigue tests on welded web attachments were summarized in NCHRP Report 227 (9). All of the available test data were acquired under constant cycle loading conditions. The results of those studies indicated that the fatigue resistance was reasonably defined by Categories E and E' depending on the attachment geometry and attachment thickness. Figure 19 includes a summary of the available constant cycle test data on welded web attachments.

During the cyclic loading of the beams tested in this study, cracking was observed to initiate at the toe of the transverse fillet weld joining the gusset to the web or the end of the longitudinal weld termination when the welds were not wrapped around the ends of the welded attachment. This was the point of greatest stress range and stress concentration due to the geometry of the fillet-welded connection, and the site of microscopic discontinuities at the weld toe. Cracks normally formed in the weld toe region, as shown in Fig. 20 and propagated into the web.

Figure 21 shows the growth of typical fatigue cracks into the girder web. In this particular case, due to the fabricator's placement of the web attachments on each web face, fatigue cracks were observed to form on two distinct planes, one from each side of the web. These can be seen in Fig. 21 where semielliptical surface cracks are apparent from each surface of the web.

Figure 22 shows another consequence of the gussets' placement on each web surface. In this case, the fatigue cracks that formed on one side of

the web propagated through the web and the weldments at the end of the attachment on the other side of the web. One semielliptical surface crack can be seen to have also propagated into the edge of the gusset plate on the opposite side of the web.

A more typical condition is shown in Fig. 23. Here the crack formed on one side of the web and propagated through the web penetrating adjacent to the weld toe on the opposite side forming a through crack. After further cracking up and down the web, the through crack was arrested by drilling holes at the end of the crack. The surface of one such hole can be seen in the lower portion of Fig. 23.

The experimental data acquired from the web attachments are summarized in Fig. 19 and compared with the Category E and E' fatigue resistance curves also shown in Fig. 19. All of the web attachments that were tested either equaled or exceeded the fatigue resistance provided by Category E' or a straight line extension of E' beyond the constant amplitude fatigue limits on a plot of effective stress range versus life.

The exceedance levels of the web attachments are summarized in Table 1 for Categories E and E'. The actual constant cycle fatigue limit is not well defined for web attachments. The value of 18 MPa (2.6 ksi) assigned Category E' is based on a fracture mechanics model of a cover plated beam (13).

Category E' was the expected resistance condition based on the constant cycle test data which is also summarized in Fig. 19. The 9 mm (0.358 in.) web thickness and attachment size of the web details provided a Category E' condition. When the effective stress range for the applied

stress range spectrum was below the constant amplitude fatigue limit, fatigue cracking still developed when a portion of the random variable loading spectrum exceeded the constant amplitude fatigue limit.

FATIGUE BEHAVIOR OF WELDED COVER PLATES

The only known fatigue data for welded cover-plated beams subjected to random variable amplitude loading were summarized in NCHRP Report 188 (1). Only six data points at $S_{rRMC} = 20.7$ MPa (3.0 ksi) and at 31 MPa (4.5 ksi) were acquired in the NCHRP 188 test program [$S_{rRMC} = 15$ MPa to 29 MPa (2.2 ksi to 4.2 ksi)]. The remainder of the data is above $S_{rRMC} = 31$ MPa (4.5 ksi). The results of those studies indicated that the fatigue resistance was reasonable defined by Category E. Figure 24 includes a summary of previous variable amplitude test data on welded cover plates.

In this test program, two cracking mechanisms were observed. In all cases the cracking occurred at the cover plate ends perpendicular to the direction of bending stress in the flange. When the cover plates were attached to the flange with longitudinal welds only, cracking was observed at the termination of the weld in the form of a semielliptical surface crack. Figure 25 shows such a crack at the longitudinal weld termination. When allowed to grow, this crack would develop into a through thickness crack as shown in Fig. 26. In some cases, several cracks would develop on different planes at this weld termination and eventually grow into one larger semielliptical crack, as shown in Fig. 27.

The cracking mechanism is different for cover plates attached to the flange with a transverse weld in addition to the longitudinal welds. In

this case, the transverse weld provides a multiplicity of initiation sites, and crack growth takes the form of several small semielliptical cracks coalescing into one long edge crack along the cover plate end at the transverse weld toe. Figures 28 and 29 show typical examples of such cracking at relatively small surface cracks.

The experimental data acquired from the sixteen cover plate details are summarized in Fig. 30. The first column of symbols represents first observed cracking, while the second column represents severing of the flange. All of the cover-plated beams tested equaled or exceeded the fatigue resistance (defined by severing of the flange) provided by Category E'.

Only two details on one beam failed at the Category E' resistance curve. Four details were observed to fail at cycle lives bounded by the Category E' and E curves. The remaining ten details exceeded the lower limit provided by Category E. The test results exceedance levels corresponded to between 0 and 10.16% of the cycles exceeding the Category E fatigue limit. No major trends were apparent that depended on the exceedance level. About the same behavior was observed when one in a thousand cycles exceeded the threshold as when one in ten exceeded it.

The results in general were comparable and consistent with the results reported in NCHRP Report 188 (1) for tests run at higher effective stress range levels.

The two cover-plate details on Beam B1 were subjected to a stress range spectrum which contained no stress ranges exceeding the constant amplitude fatigue limit. After one hundred million total cycles, no

visible cracking was observed. However, after destructively examining the details, two of the cover plate ends were discovered to contain very small semielliptical cracks [$a = 1 \text{ mm (0.04 in.)}$], as shown in Figs. 31 and 32. These cracks were estimated to require an additional 100 million cycles to sever the flange.

One other crack was discovered destructively on Beam C2 after 10.7×10^6 cycles. An estimated 32.3×10^6 variable stress cycles were predicted before the flange was severed on this beam. Beam D1 was subjected to between 60-70 million additional cycles after cracking was detected and the flanges were severed. This confirmed the adequacy of the estimated residual life based on the observed crack sizes and the effective stress range.

FATIGUE CRACK GROWTH UNDER RANDOM VARIABLE LOADING

The Amsler Vibrophore was used to acquire the fatigue crack growth test data. A ten ton dynamometer was used and allowed a maximum load of 98.5 kN (22 kips) tension. The random block loading was controlled by a solid state storage device and clock that controlled the length of time of each individual stress block. Prior to applying the random loading, the cracks were started under constant cycle loading in order to provide a sharp initial crack condition. Friction grips were used to hold the specimen in the machine. Strain gages were mounted on the surface of each specimen in order to monitor the cyclic stress and insure that no bending gradients were introduced into the specimen.

The cyclic test parameters used for the various random variable block loading is summarized in Table 2. Data was recorded at selected intervals by recording the number of cycles of load and the crack length. Tables A3 - A6 in Appendix A give the crack size, S_{rRMC} and the elapsed stress cycles.

The test results were evaluated by relating the average rate of fatigue crack growth, da/dN , under the random variable block loading to the root-mean-cube of the stress intensity factor fluctuation ΔK_{RMC} . The value of ΔK_{RMC} was directly estimated from the effective stress range for the variable cyclic stress spectrum.

The results of the test data evaluation are summarized in Fig. 33. Also shown is the upper bound crack growth relationship

$$\frac{da}{dN} = 3.6 \times 10^{-10} \Delta K^3 \quad (5)$$

suggested by Barsom and Rolfe for constant amplitude test data of ferrite-pearlite steel (9). This relationship has been extended below the constant cycle crack growth threshold which is dependent on the R ratio. At high R ratios, this value approaches $3.3 \text{ MPa } \sqrt{\text{m}}$ ($3 \text{ ksi } \sqrt{\text{in.}}$).

The results of da/dN and ΔK_{RMC} were compared with the upper bound crack relationship suggested by Rolfe and Barsom (10) in Fig. 34. The comparison given in Figs. 33 and 34 demonstrated that the effective stress intensity range ΔK_{RMC} is in good agreement with the relationship derived from Eq. 2.

The random variable crack growth relationship was observed to correlate with the extrapolation of Eq. 5 to crack growth rates below the constant cycle crack propagation threshold, ΔK_{th} .

The test data plotted in Fig. 34 is compared with the scatterbands observed by Klingerman and Barsom (11,5). The random variable crack growth threshold can be seen to be sensitive to the R-ratio, just as was observed with constant cycle tests.

The crack growth behavior of the upper and lower crack were directly comparable as was the data acquired from ΔK decreasing and ΔK increasing. This can be seen in Fig. 35 for the R = 0.55 test specimen.

Several constant amplitude crack growth tests were carried out on the A36 steel plate material for comparative purposes near the crack growth threshold. The procedures suggested in Refs. 6 and 7 were used to evaluate the crack growth threshold. The test results are summarized in Fig. 36. For an R-ratio of 0.8, a threshold was observed at $K = 3.8 \text{ MPa } \sqrt{\text{m}}$ (3.5 ksi $\sqrt{\text{in.}}$). R-ratio of 0.3 and 0.55 gave a crack growth threshold of about $6 \text{ MPa } \sqrt{\text{m}}$ (5.5 ksi $\sqrt{\text{in.}}$). These results are near the upper bound of the crack growth threshold described by Barsom and Novak (5).

As can be seen in Table 2, only a relatively small percentage of the random variable block stress cycles resulted in stress intensity factor ranges which exceed the constant cycle crack growth threshold. Nevertheless, this resulted in fatigue crack growth and a significant lowering of the crack growth threshold. At the 0.8 R-ratio, the threshold was reduced

from 3.8 MPa \sqrt{m} (3.5 ksi $\sqrt{in.}$) to about 2.2 MPa \sqrt{m} (2 ksi $\sqrt{in.}$). At an R-ratio of 0.55, the threshold decreased from 6 MPa \sqrt{m} (5.5 ksi $\sqrt{in.}$) to about 3.8 MPa \sqrt{m} (3.5 ksi $\sqrt{in.}$).

FATIGUE BEHAVIOR OF NONLOAD-CARRYING WELDS

UNDER RANDOM VARIABLE BLOCK LOADING

The Amsler Vibrophore was used to acquire fatigue test data of the nonload-carrying fillet welds under a bending type loading, as illustrated in Fig. 17. Crack growth was possible at either of the two weld toes that were perpendicular to the stress field. Figure 18 shows the configuration of the surface cracks that were observed to form under constant and variable loading in these specimens.

The available constant cycle test data on similar bending specimens are compared with the results obtained in this test program in Fig. 37. The crosses represent test data from Refs. 20 and 21 on structural carbon steel (ST37 and A36) and on high strength low alloy steel (ST52). It is readily apparent that these small specimens provide wide variations in fatigue resistance with the test data extending from the lower bound Category C line to beyond Category B. The five test results represented by the tests on A514 steel are indicated by the crossed circle. All of the tests are seen to fall near the upper bound of the test data from Refs. 20 and 21. The specimen tested at a stress range of 152 MPa (22 ksi) sustained 62×10^6 cycles with no detectable crack growth at the weld toes.

The variable amplitude test data are plotted in Fig. 38 as crosses. It can be seen that they also provided fatigue resistances that were at or

above Category B. Only two specimens plotted near the Category B line, and most specimens exceeded it by a large margin. One specimen tested at an effective stress range of (17.7 ksi) and one at a stress range of (23.7 ksi) did not exhibit any crack growth after 10^8 cycles, and testing was discontinued. These specimens were subsequently broken apart, and no evidence of crack growth was observed.

Also plotted in Fig. 38 are the results obtained on direct tension specimen by Albrecht⁽²⁾. These variable load tests also yielded fatigue resistances that were near Category B. Both submerged arc and manually made welds provided fatigue resistances that were greater than the resistance of similar details attached to beam specimens. The small simulated specimens subjected to variable loading appear to provide slightly greater fatigue resistance when compared with the constant cycle specimens than do the beam details.

4. CONCLUSIONS AND APPLICATION OF RESULTS

The results obtained from these variable amplitude tests are consistent with the previously reported constant amplitude tests (9,12,13,14). However, the existence of a fatigue limit below which no fatigue crack propagation occurs is assured only if none of the stress range cycles exceed this constant amplitude fatigue limit. If any of the stress range cycles (as few as one per thousand cycles) exceed the constant cycle fatigue limit, crack propagation will likely occur. In this study, the percentage of cycles exceeding the previously defined constant amplitude fatigue limit was varied from 0.10% to 11.72%. In all of these cases, fatigue crack propagation occurred.

Two of the cover-plated details were subjected to a stress range spectrum which contained no stress ranges exceeding the constant amplitude fatigue limit. Even in these two cases, limited crack propagation occurred. This likely resulted because the constant cycle fatigue limit is not precisely defined. The test reported in Ref. 3 indicated that the constant cycle limit may be 1.4 to 2.1 MPa (0.2 - 0.3 ksi) lower than the value of 35 MPa (5 ksi) used for Category E.

Therefore, for the fatigue analysis of details subjected to variable amplitude loading (e.g. highway and railroad bridges), two parameters must be considered, the effective stress range and maximum stress range. Three different situations can be encountered:

1. Effective Stress Range > Constant amplitude fatigue limit
2. Effective Stress Range < Constant amplitude fatigue limit
Maximum Stress Range > Constant amplitude fatigue limit
3. Effective Stress Range < Constant amplitude fatigue limit
Maximum Stress Range < Constant amplitude fatigue limit

As shown in Fig. 39, the S-N curves developed for details subjected to constant amplitude loading can be used to estimate the fatigue life of details subjected to variable amplitude loading. For Case 1 in which the effective stress range S_{rRMC} is greater than the constant amplitude fatigue limit, this effective stress range is used as the constant amplitude stress range in conjunction with the constant amplitude S-N curve to determine fatigue life. In Case 2, the effective stress range is below the constant amplitude fatigue limit, yet the maximum stress range exceeds this limit; therefore, the effective stress range must be utilized in conjunction with a straight line extension of the sloping portion of the constant amplitude S-N curve to determine life. For Case 3, since all of the stress range spectrum is below the constant amplitude fatigue limit, none of the stress ranges should be damaging, and no fatigue crack propagation is expected.

The results of this investigation verify the assumption made in Ref. 19 that the S-N curves developed for details subject to constant amplitude loading can be used to predict the fatigue life of details subjected to variable amplitude loading. This assumption was also used to develop the extreme life loading condition in the AASHTO and AREA

specifications. Further, the results can be used to assess the potential fatigue damage at bridge details if the nature of the stress spectrum is known as a result of normal truck traffic and known overloads. The damage due to permit loads that cause stress cycles to exceed the constant amplitude fatigue limit can be approximately ascertained. Care must be exercised when estimating the magnitude of cyclic stress as the load distribution and impact are not likely to be as severe as used in the design calculations.

5. RECOMMENDATIONS FOR FURTHER RESEARCH

- (1) In order to provide a larger, more comprehensive data base, additional full-scale random variable amplitude beam tests similar to those tested in this test program are required.

The primary parameters under investigation are the root-mean-cube effective stress range of skewed (i.e., Rayleigh-type) variable amplitude load distribution

$$S_{re} = \Sigma (\alpha_i S_{ri}^3)^{1/3}$$

and the percentage of the loadings in the spectrum which exceed the constant amplitude fatigue limit. Effective stress ranges between 13.8 MPa and 27.6 MPa (2 ksi and 4 ksi) have been examined in this study with exceedances above the Category E or E' constant cycle fatigue limit varying between 0.1% and 12% of the total accumulated stress cycles.

Other than the studies reported in NCHRP Report 188 (1), the small specimens reported by Albrecht (2) and the specimens summarized by Tilly and Nunn (4), no other test data are known to be available particularly at the lower stress range levels.

More such tests need to be run at lower values of the root-mean-cube effective stress range to accurately assess the relationship between fatigue life and effective stress range under random loading. The effect of exceedance of the constant amplitude fatigue limit

appears to be more severe than predicted when beam specimens are used. Therefore, more tests should be run with very small percentages of the load spectrum exceeding the currently accepted constant amplitude fatigue limit. Based on experience acquired from these tests, many of these tests may require 10^8 random variable loadings.

- (2) Since the AASHTO Specification provisions were developed in NCHRP Report 147 (12), several major fatigue studies have been carried out on similar beam type specimens. Tests were carried out in East Germany (15), Japan (16), by the Office for Research and Experiments of the International Union of Railways (ORE - West Germany, Poland, England, Holland) (17), and here in the United States (1,18). Also, during the last several years, a Task Committee of European Convention for Constructional Steelwork (ECCS) has been developing comprehensive specification provisions using the NCHRP studies and other supplementary work. All of this material needs to be reexamined to ascertain what changes are to be made, if any, in the AASHTO Specifications and to broaden the data base. Since the ECCS drafts have been submitted to the International Organization for Standardization (ISO), it would be beneficial to examine all of this data, so that our national codes can be related to the ISO provisions. The basic ISO fatigue design relationships have been developed by creating equally spaced S-N curves between base metal and cover plate beam members.

- (3) A pilot study, on five full-scale girders, investigated for out-of-plane displacement-induced fatigue cracking, and subsequent retrofiting was included in NCHRP Project 12-15(2) (13).

Since the study reported in NCHRP Report 206 has been carried out, numerous bridge structures have been discovered with displacement induced web cracks. A recent survey has shown that cracks have formed in multiple girder bridges with diaphragms as well as the two girder-floor beam type of bridge structure. Hence, more basic fatigue data needs to be developed for the web gap region. Retrofit schemes should also continue to be examined and tested to provide confidence and direction for bridge engineers.

The only laboratory information known to exist for the web gap cracking is the pilot study reported in NCHRP Report 206. This study obtained information on the effect of gap length and the magnitude of out-of-plane displacement. The web cracked members were then subjected to cyclic loading after retrofit holes were installed. Questions have been raised on the adequateness of the data base and on its direct applicability to web cracked structures, as the web was not displaced out-of-plane during the subsequent cyclic loading. Further research into the out-of-plane displacement-induced fatigue cracking problem and methods to retrofit are necessary.

TABLE 1

Test No.	Beam No.	Web Attachments					Cover Plate Ends									
		S_{rmin}		S_{rmax}		S_{rRMC}	$\Sigma\gamma_{if}(E)$	$\Sigma\gamma_{if}(E')$	S_{rmin}		S_{rMax}		S_{rRMC}	$\Sigma\gamma_{if}(E)$		
		MPa (ksi)	MPa (ksi)	MPa (ksi)	MPa (ksi)	MPa (ksi)	(%)	(%)	MPa (ksi)	MPa (ksi)	MPa (ksi)	MPa (ksi)	MPa (ksi)	(%)		
1 W = 4.0	C1	12.1	1.75	44.8	6.5	24.1	3.5	4.69	72.58	13.1	1.9	47.6	6.9	25.5	3.7	4.69
	C2	13.8	2.0	51.7	7.5	27.6	4.0	10.16	87.81	13.1	1.9	49.0	7.1	26.9	3.9	10.16
2 W = 3.75	A1	14.5	2.1	42.7	6.2	24.8	3.6	1.76	85.93	13.8	2.0	40.7	5.9	23.4	3.4	1.76
	A2	16.5	2.4	49.6	7.2	29.0	4.2	11.72	97.20	14.5	2.1	42.7	6.2	24.8	3.6	4.90
3 W = 4.75	B1	6.2	0.9	35.9	5.2	15.2	2.2	0.10	13.85	6.2	0.9	33.8	4.9	14.5	2.1	0.0
	B2	6.9	1.0	41.4	6.0	17.9	2.6	0.49	27.14	6.2	0.9	35.9	5.2	15.2	2.2	0.10
4 W = 4.75	D1	7.6	1.1	46.2	6.7	20.0	2.9	1.07	39.81	6.9	1.0	44.1	6.4	19.3	2.8	0.49
	D2	7.6	1.1	46.2	6.7	20.0	2.9	1.07	39.81	6.9	1.0	44.1	6.4	19.3	2.8	0.49

TABLE 2

TEST VARIABLES FOR FATIGUE CRACK GROWTH STUDIES

<u>R</u>	<u>S_{rmin}*</u>	<u>S_{rmax}*</u>	<u>S_{rRMC}</u>	<u>ΔK_{min}</u>	<u>ΔK_{max}</u>	<u>ΔK_{RMC}</u>
0.8	2.50	8.04	5.04	2.55	8.19	5.13
	to	to	to	to	to	to
	0.84	2.69	1.69	1.14	3.66	2.30
0.55	2.78	8.92	5.60	5.30	17.01	10.67
	to	to	to	to	to	to
	1.32	4.23	2.65	1.96	6.30	3.95
0.30	4.07	13.08	8.21	3.90	12.53	7.86
	to	to	to	to	to	to
	2.17	6.95	4.36	2.40	7.72	4.84

*During the progress of the test the stress range was decreased in 10% increments to compensate for the increasing crack size and to approach the crack growth threshold.

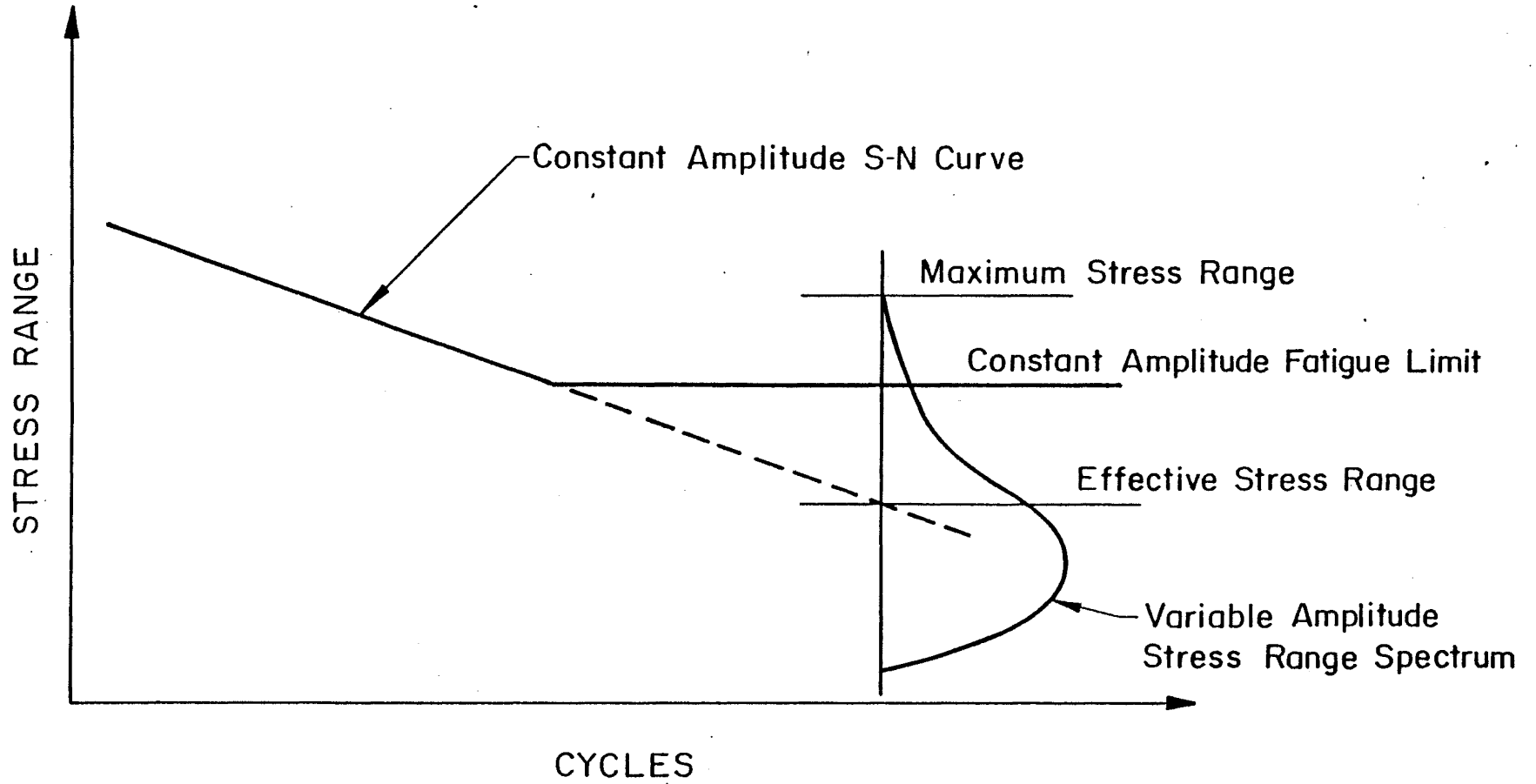


Fig. 1 Variable Amplitude Stress Range Spectrum Superimposed Over a Constant Amplitude S-N Curve

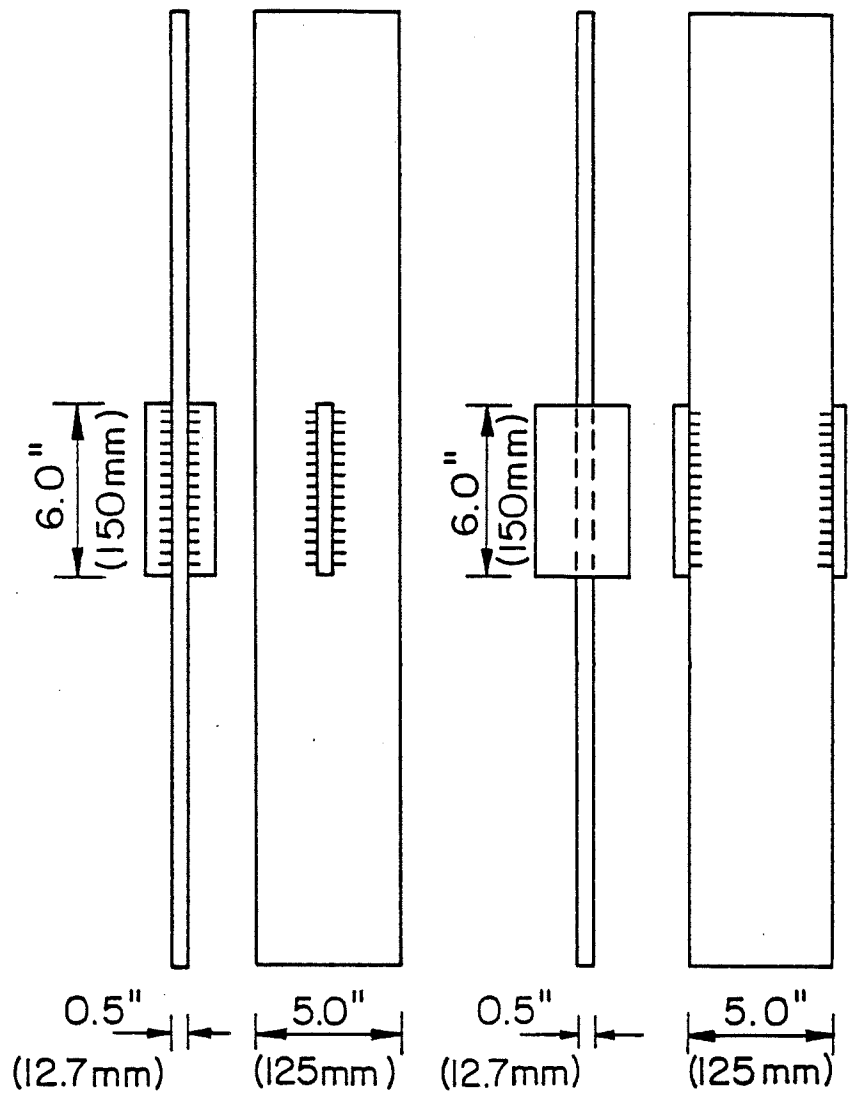


Fig. 2 Tilly and Nunn Test Specimens

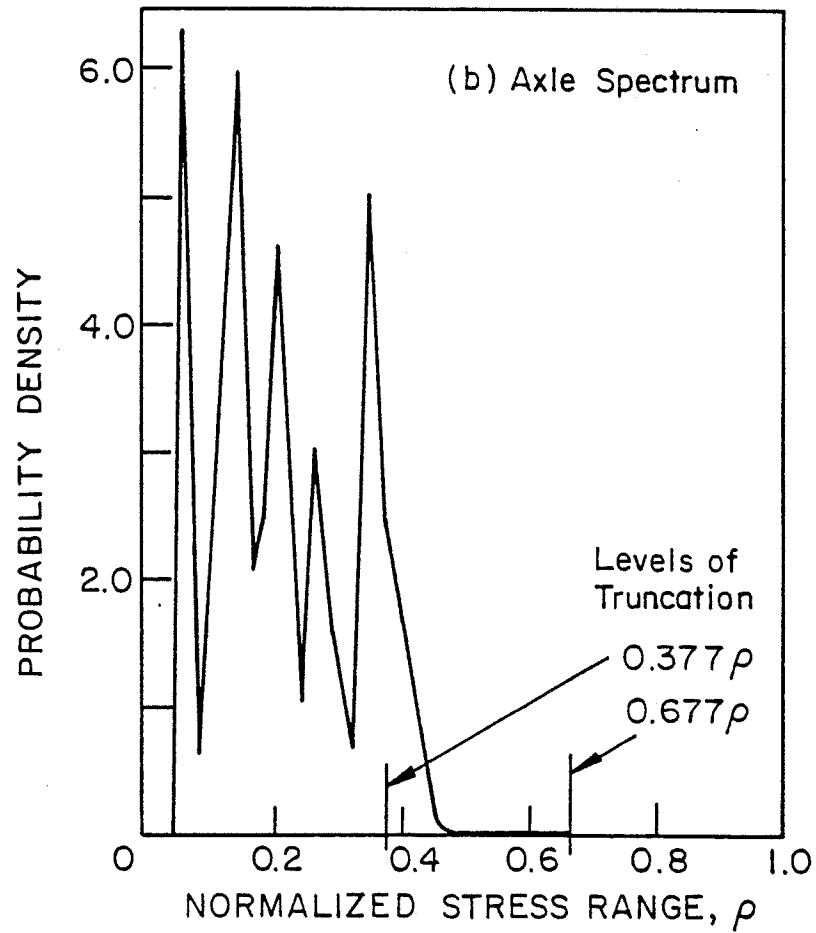
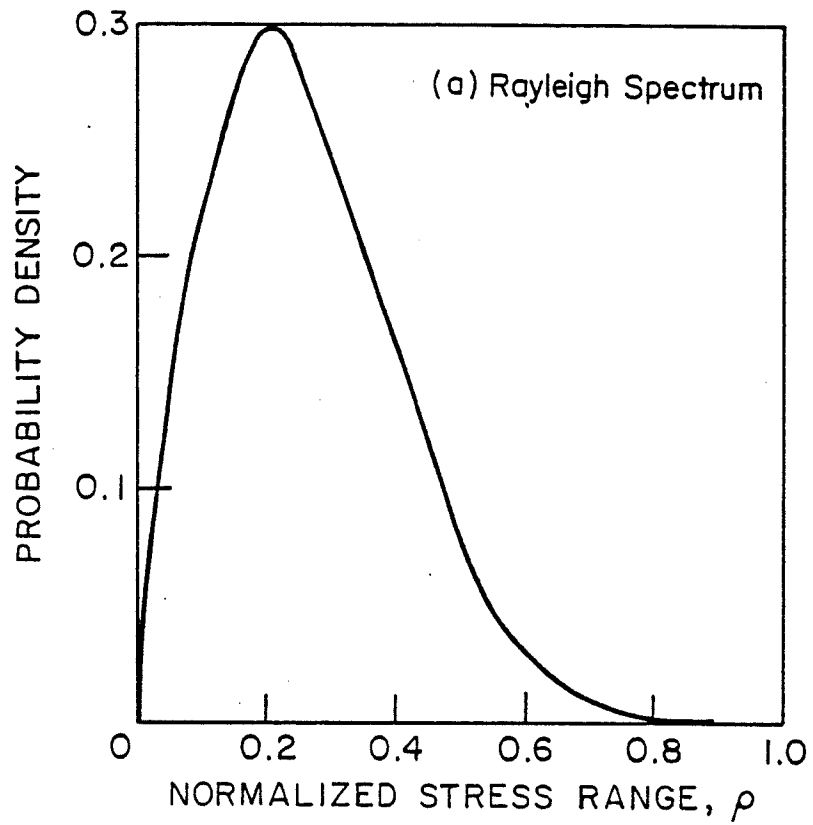
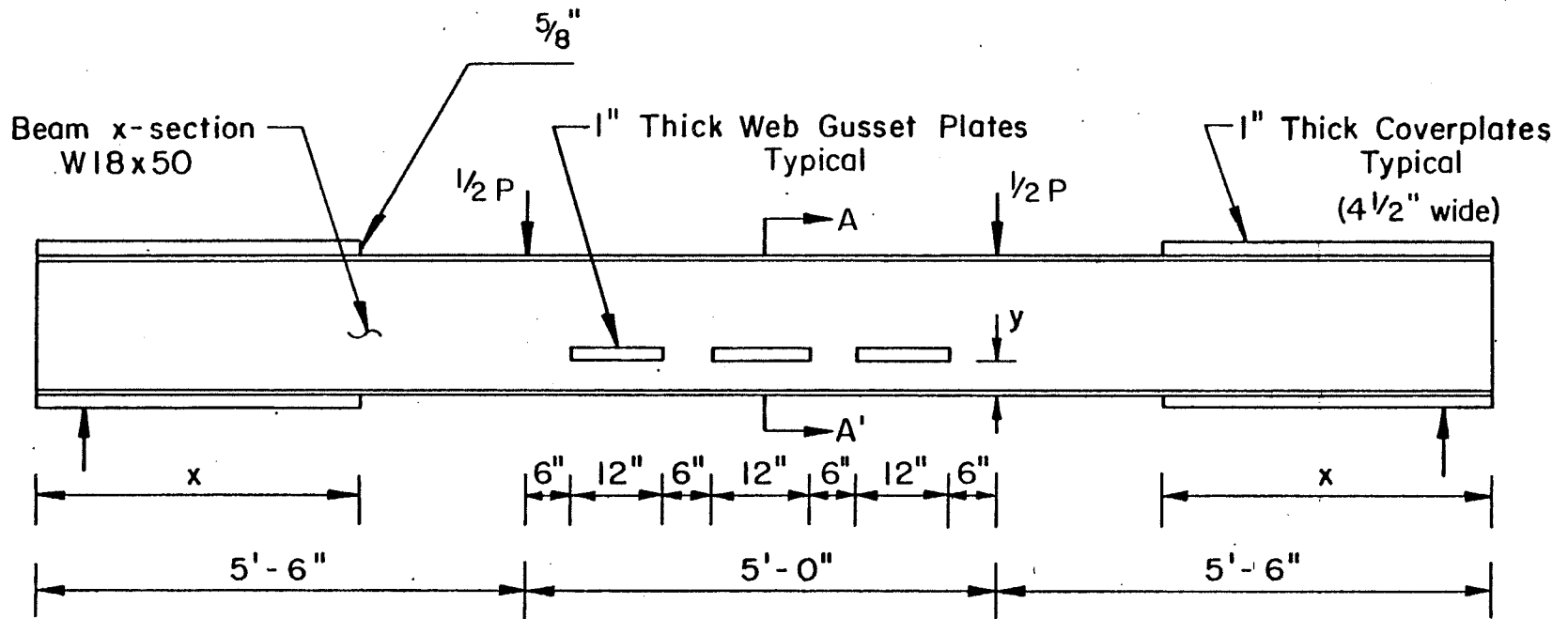
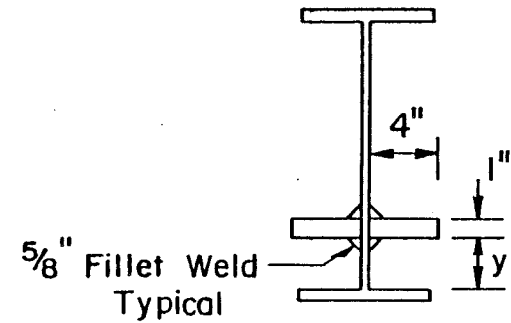


Fig. 3 Tilly and Nunn Stress Range Spectra



Note: distance y measured from top of bottom flange to bottom of web gusset

No. of Beams	y (inches)	x (inches)
4	2"	46 $\frac{3}{4}$ "
2	2 $\frac{1}{4}$ "	45 $\frac{1}{8}$ "
2	2 $\frac{7}{8}$ "	41 $\frac{1}{4}$ "
2	3 $\frac{1}{8}$ "	39 $\frac{1}{2}$ "



Section A-A

Fig. 4 Test Beams

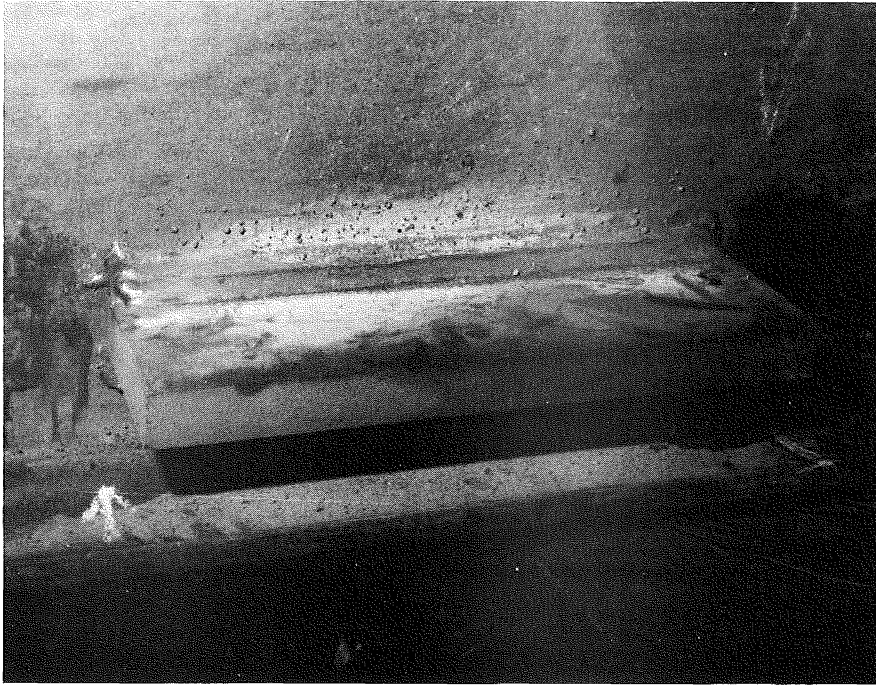


Fig. 5 Gusset Plate Fillet Welded to Web
in Constant Moment Region

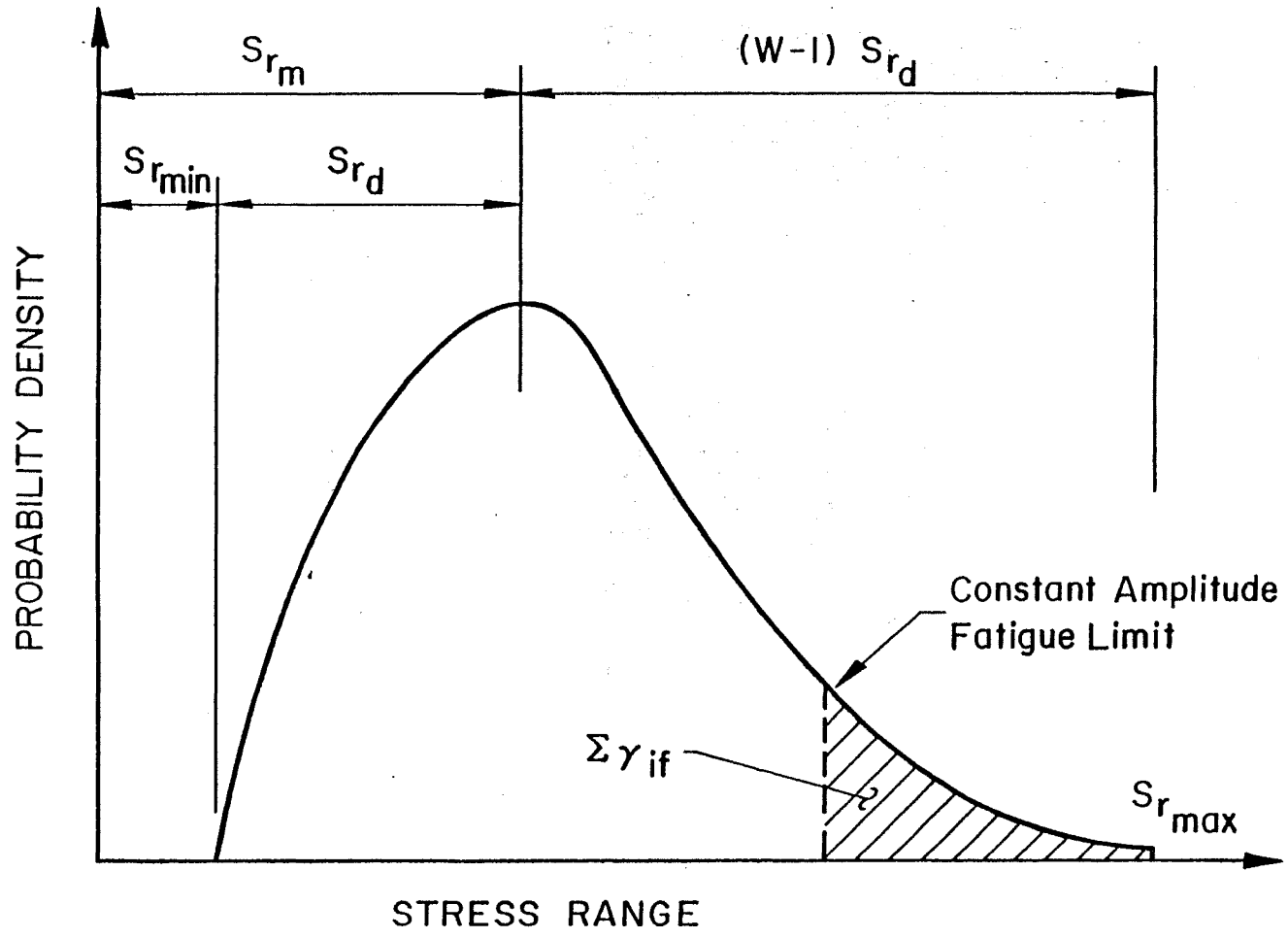


Fig. 6 Rayleigh-type Stress Range Spectrum

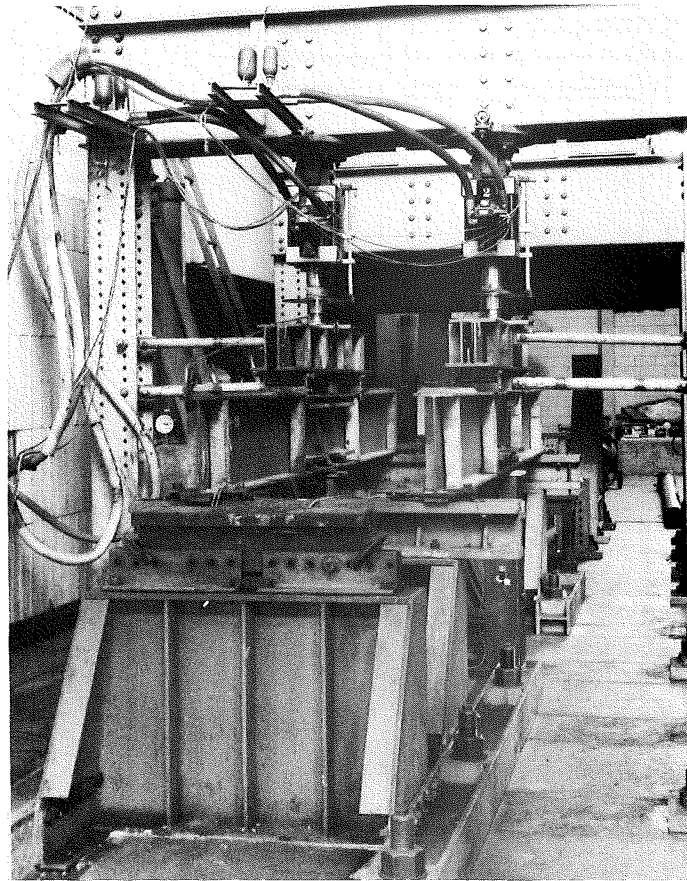


Fig. 7 Test Beams on Dynamic Test Bed

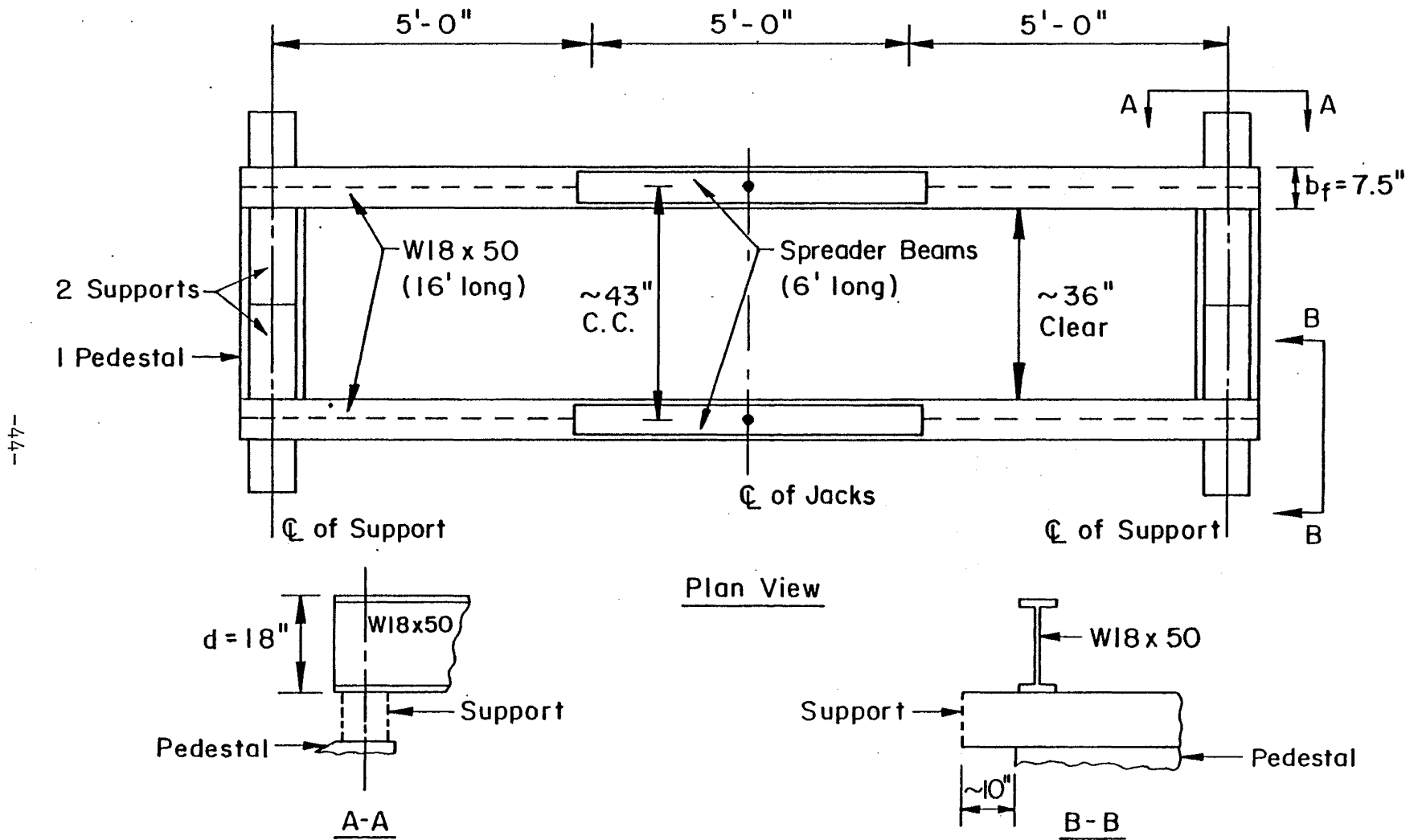


Fig. 8 Plan View of Test Setup

Test No. 3
Beam No. B2
Web Attachment

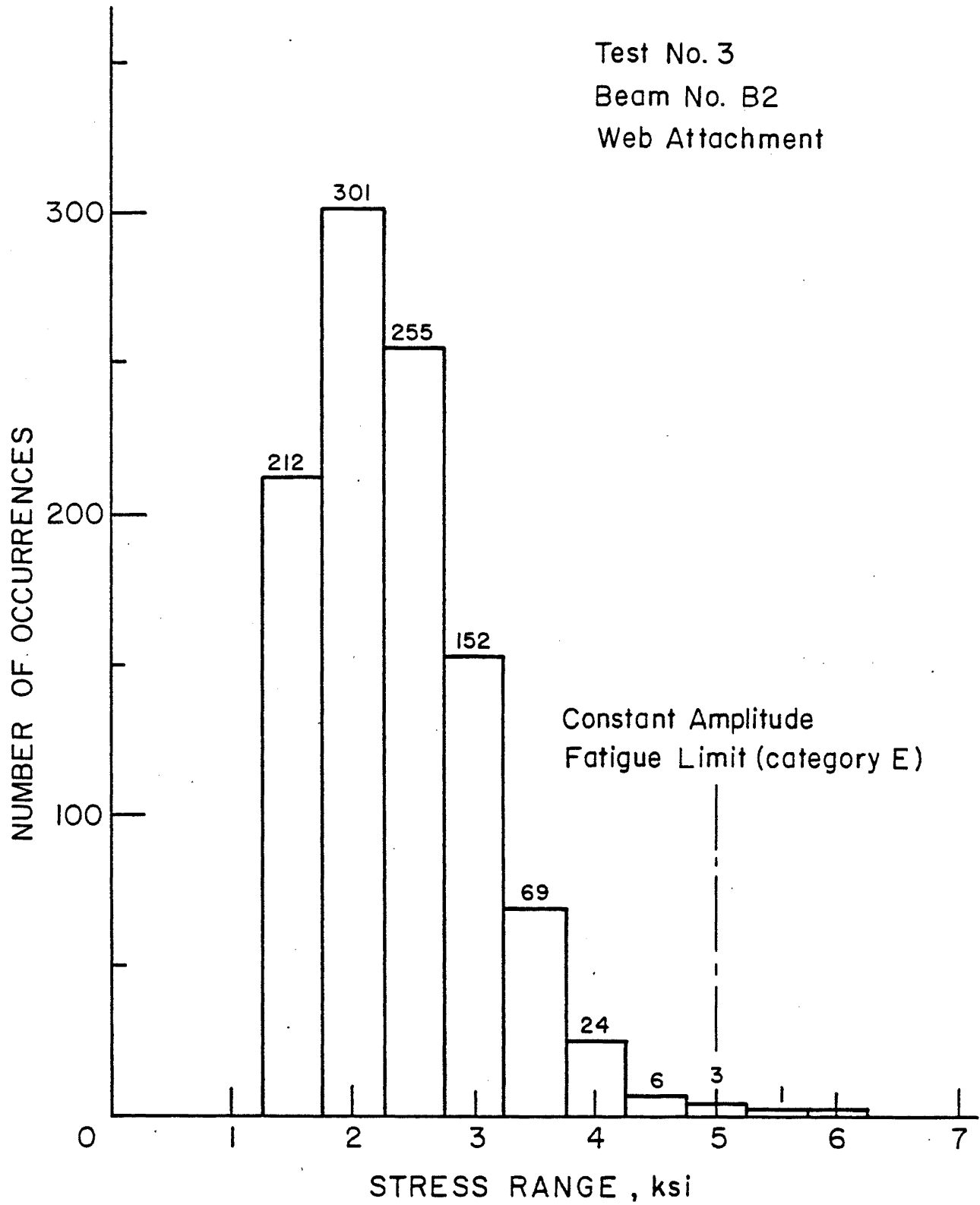


Fig. 9 Simulated Variable Amplitude Stress Range Spectrum

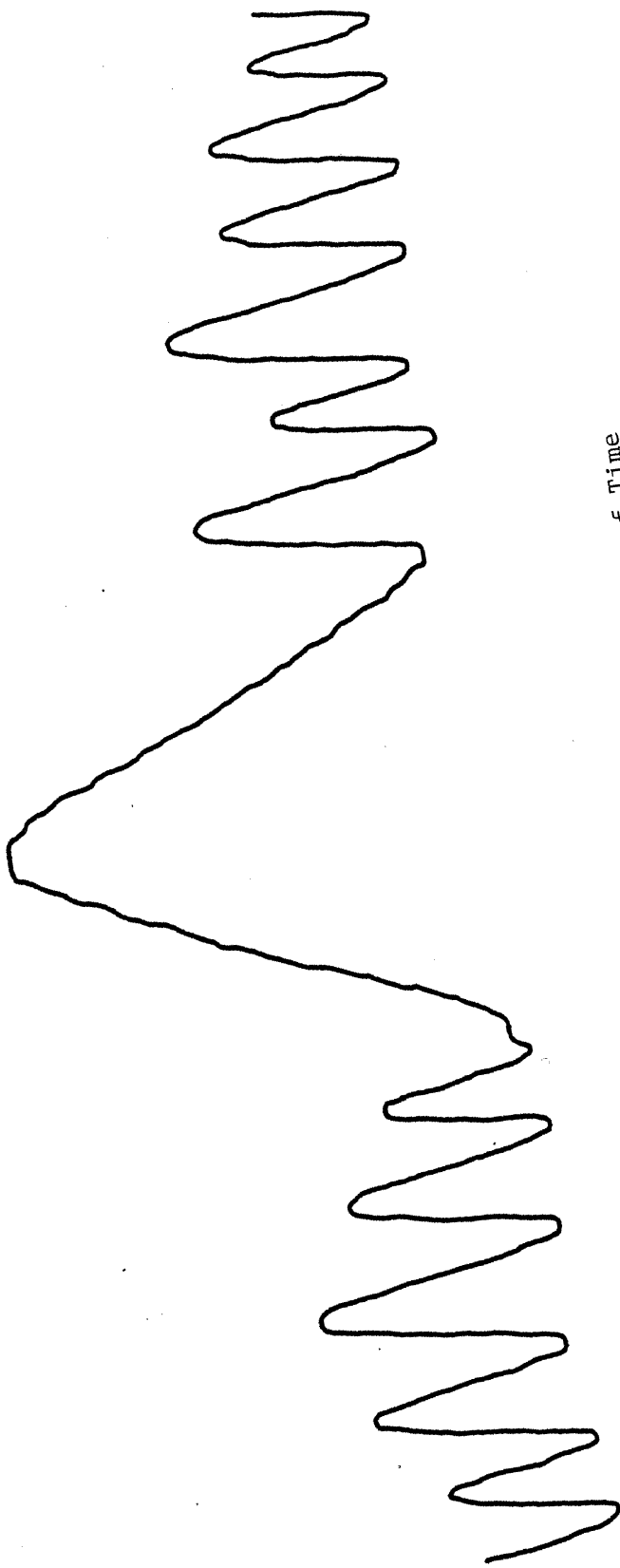


Fig. 10 Stress Range as a Function of Time

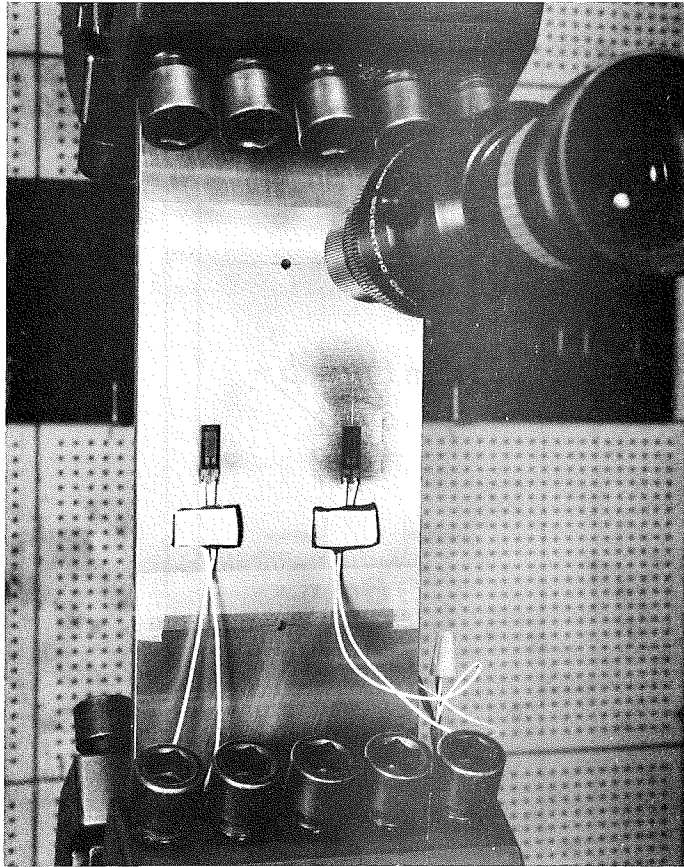


Fig. 11 Fatigue Crack Growth Specimen in Test Setup

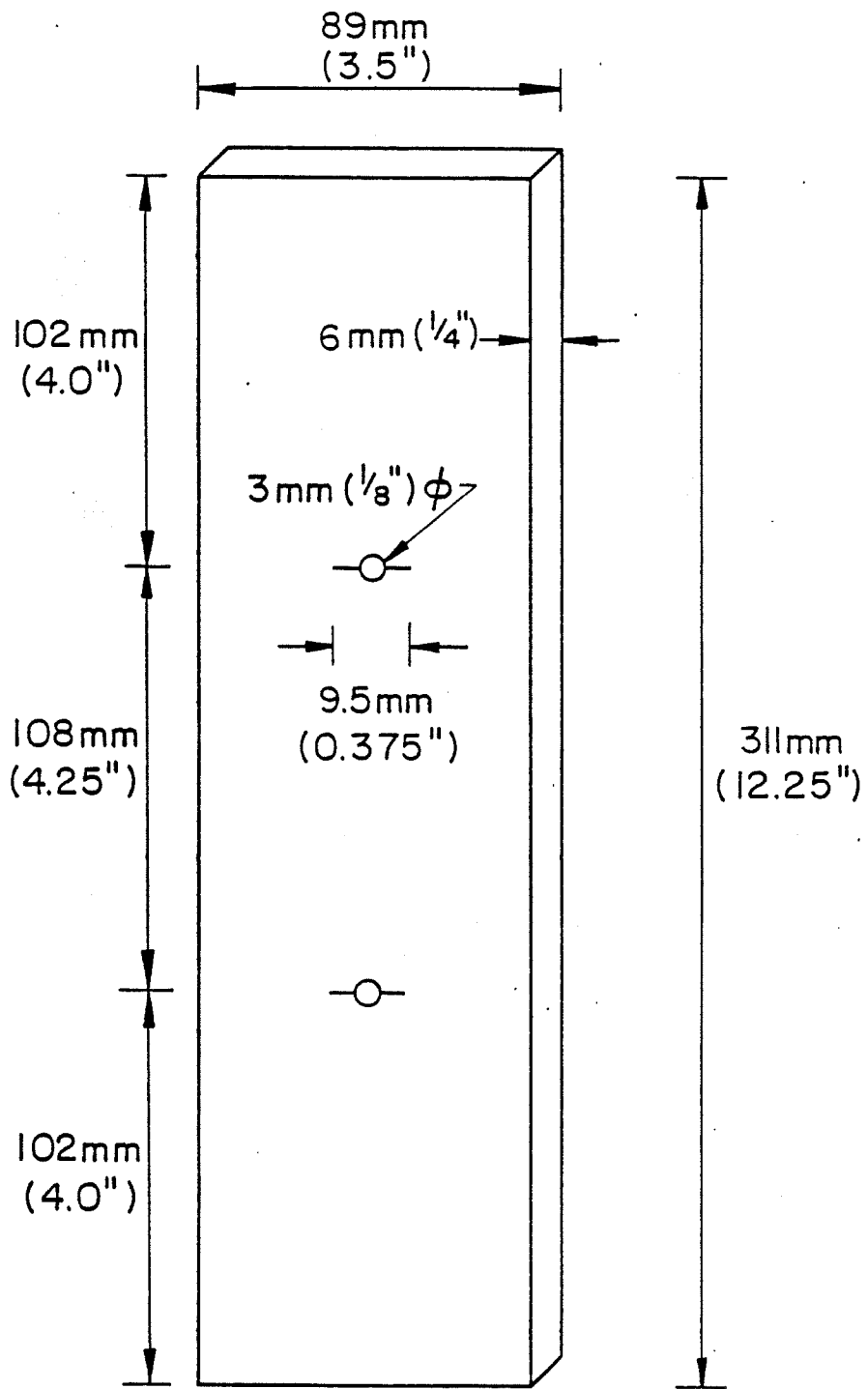


Fig. 12 Fatigue Crack Growth Specimen

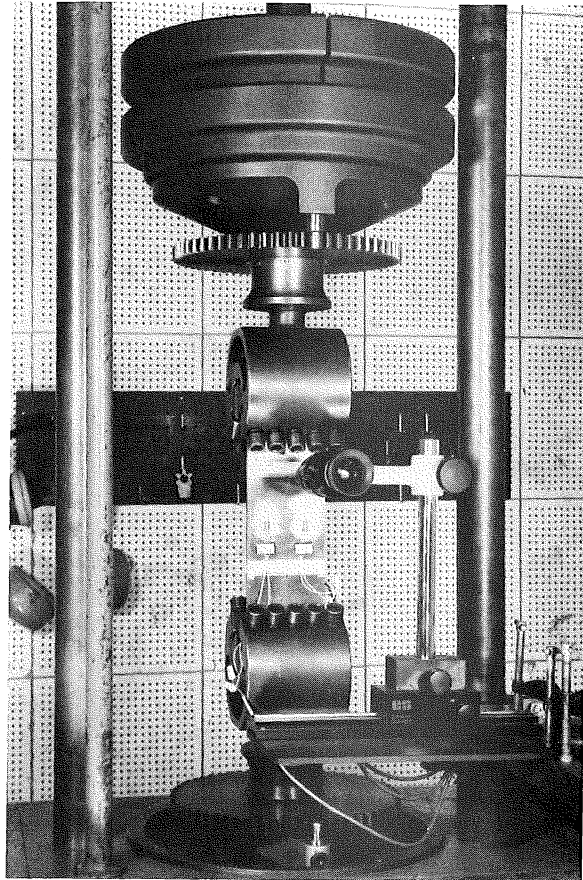


Fig. 13 Fatigue Crack Growth Test Setup

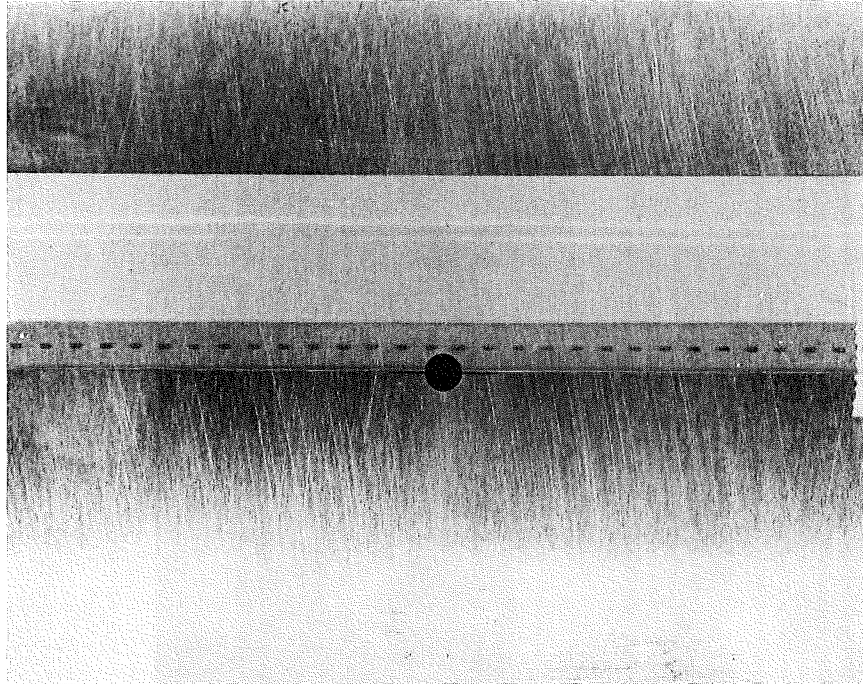


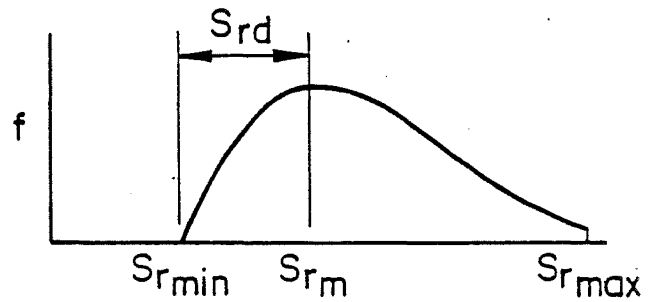
Fig. 14 Mylar Tape Attached to Plate Surface

Variable Amplitude Loading

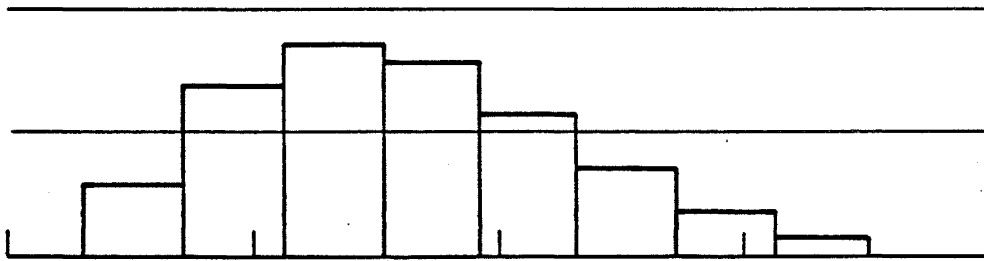
Rayleigh Distribution

$$\frac{S_{rd}}{S_{rm}} = 0.5$$

$$w = \frac{S_{rmax} - S_{rmin}}{S_{rd}} = 3$$



Histogram



No. of stress levels :	8
No. of blocks :	150
No. of cycles in a block :	960
No. of cycles in a period :	1.444×10^5

Fig. 15 Fatigue Crack Growth Study Stress Spectrum

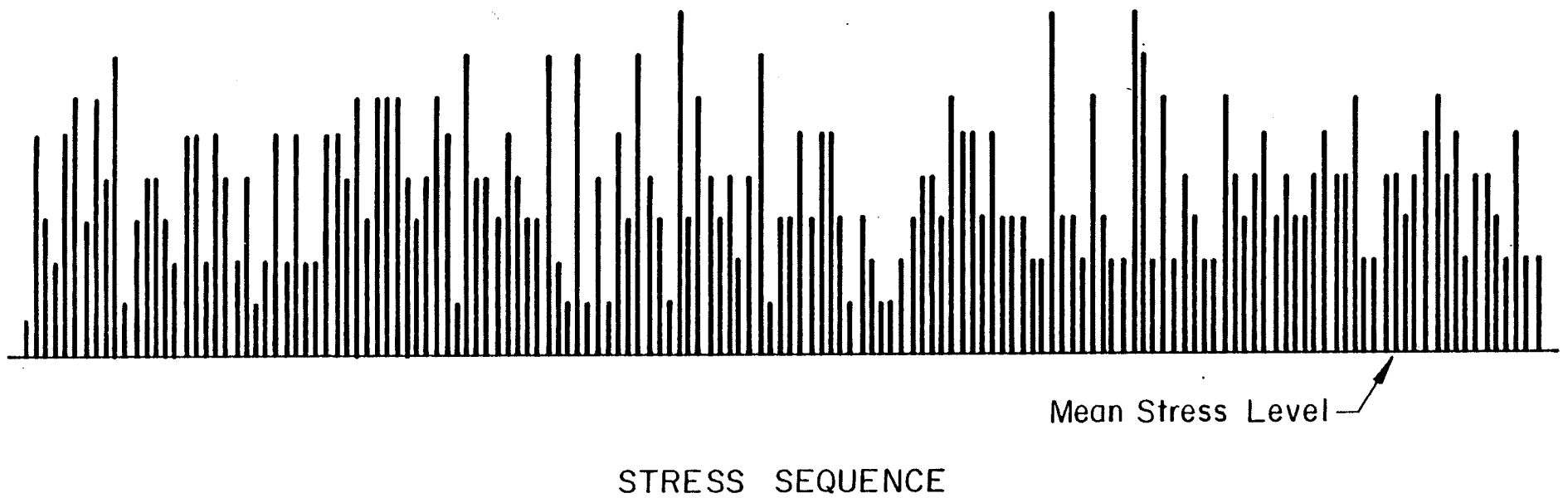


Fig. 16 Randomized Stress Block Sequence

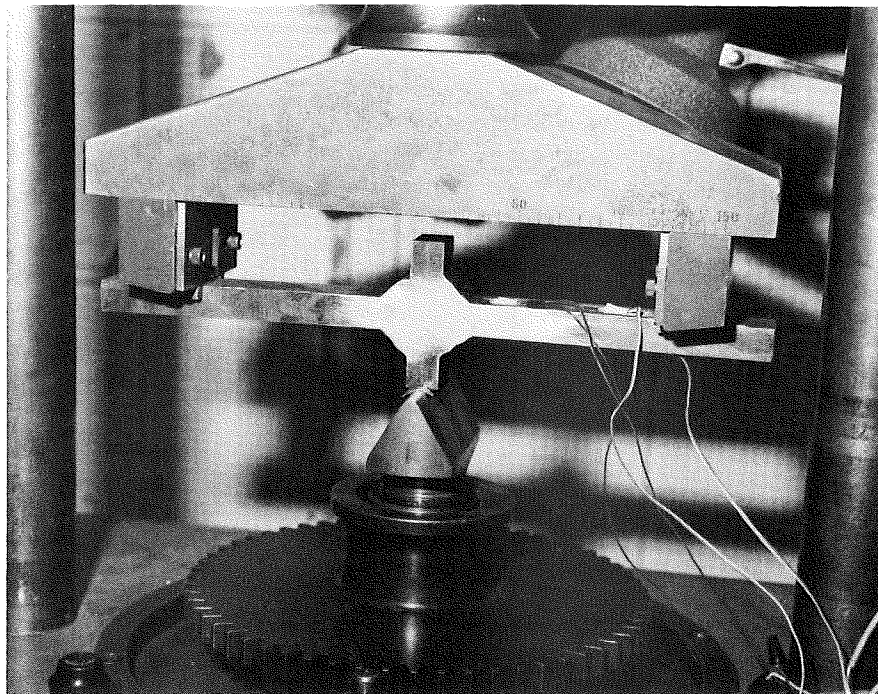


Fig. 17 Cruciform Type Specimen in Test Setup

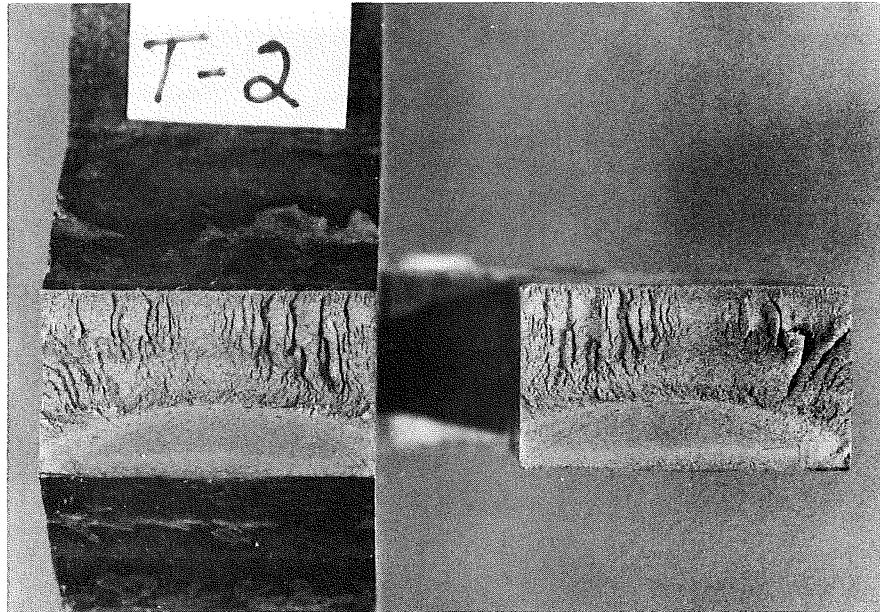


Fig. 18 Typical Cruciform Specimen Crack Surface

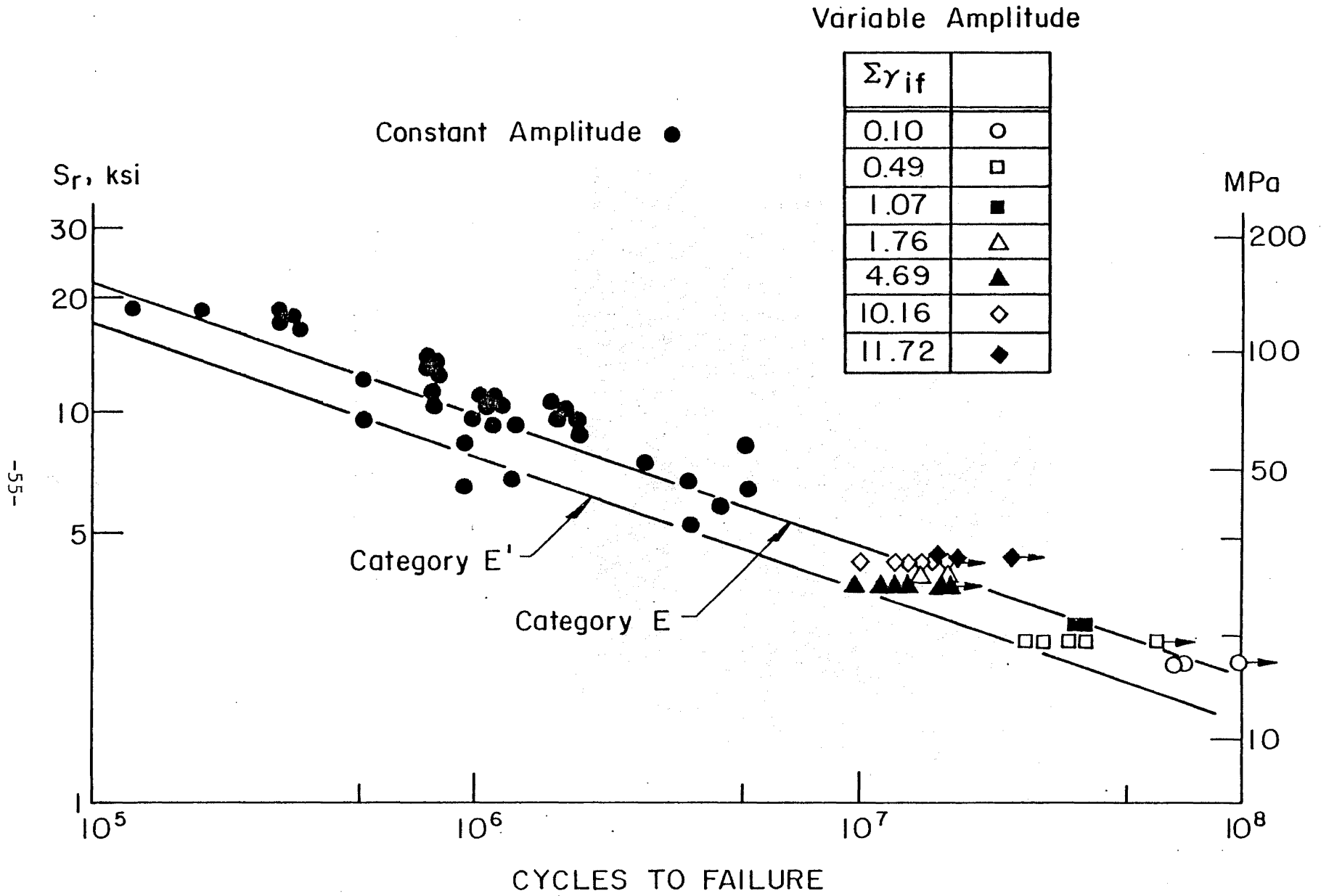


Fig. 19 Web Attachment Experimental Data

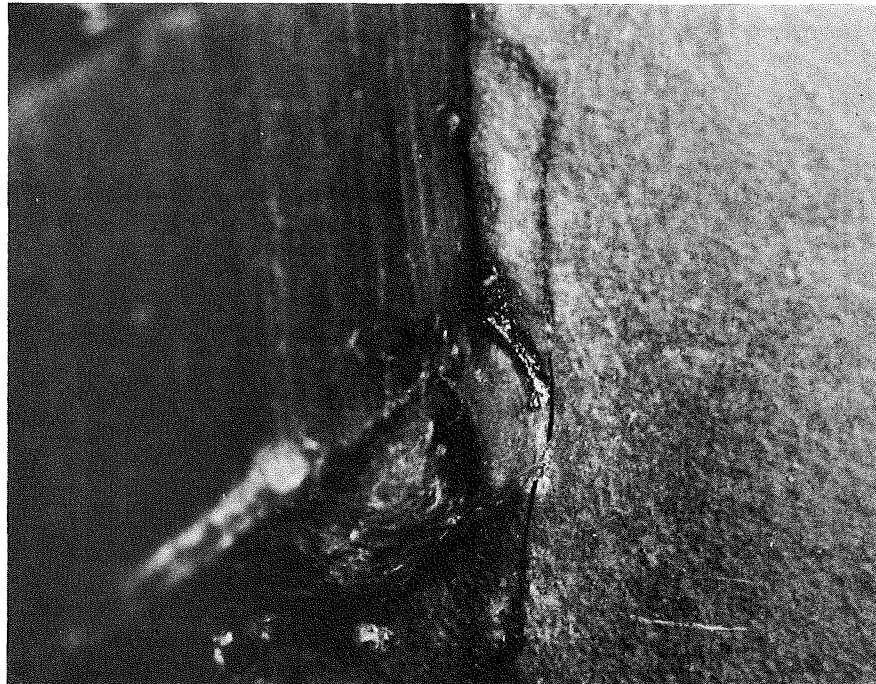


Fig. 20 Typical Surface Crack at Weld Toe
of Web Attachment



Fig. 21 Typical Fatigue Crack Development
at Web Attachment
(Beam B3 - East Attachment)

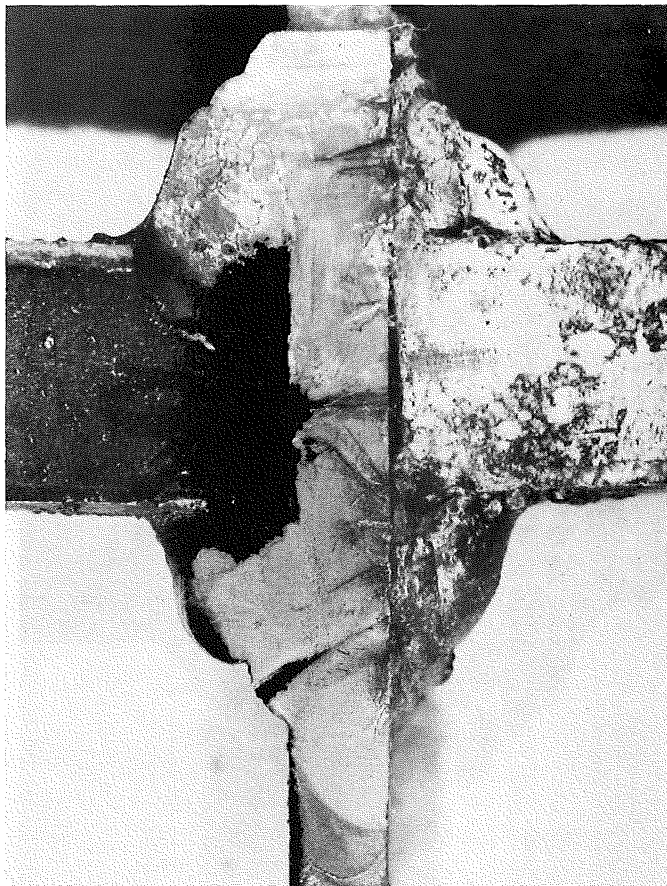


Fig. 22 Typical Fatigue Crack Development
at Web Attachment
(Beam C2 - East Attachment)

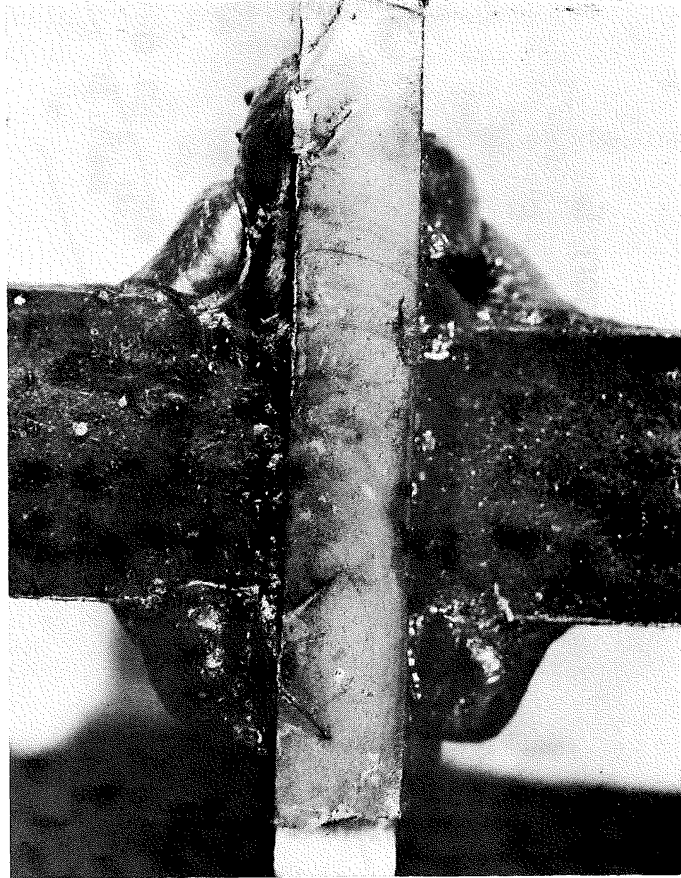


Fig. 23 Typical Fatigue Crack Development
at Web Attachments
(Beam C1 - Middle Attachment)

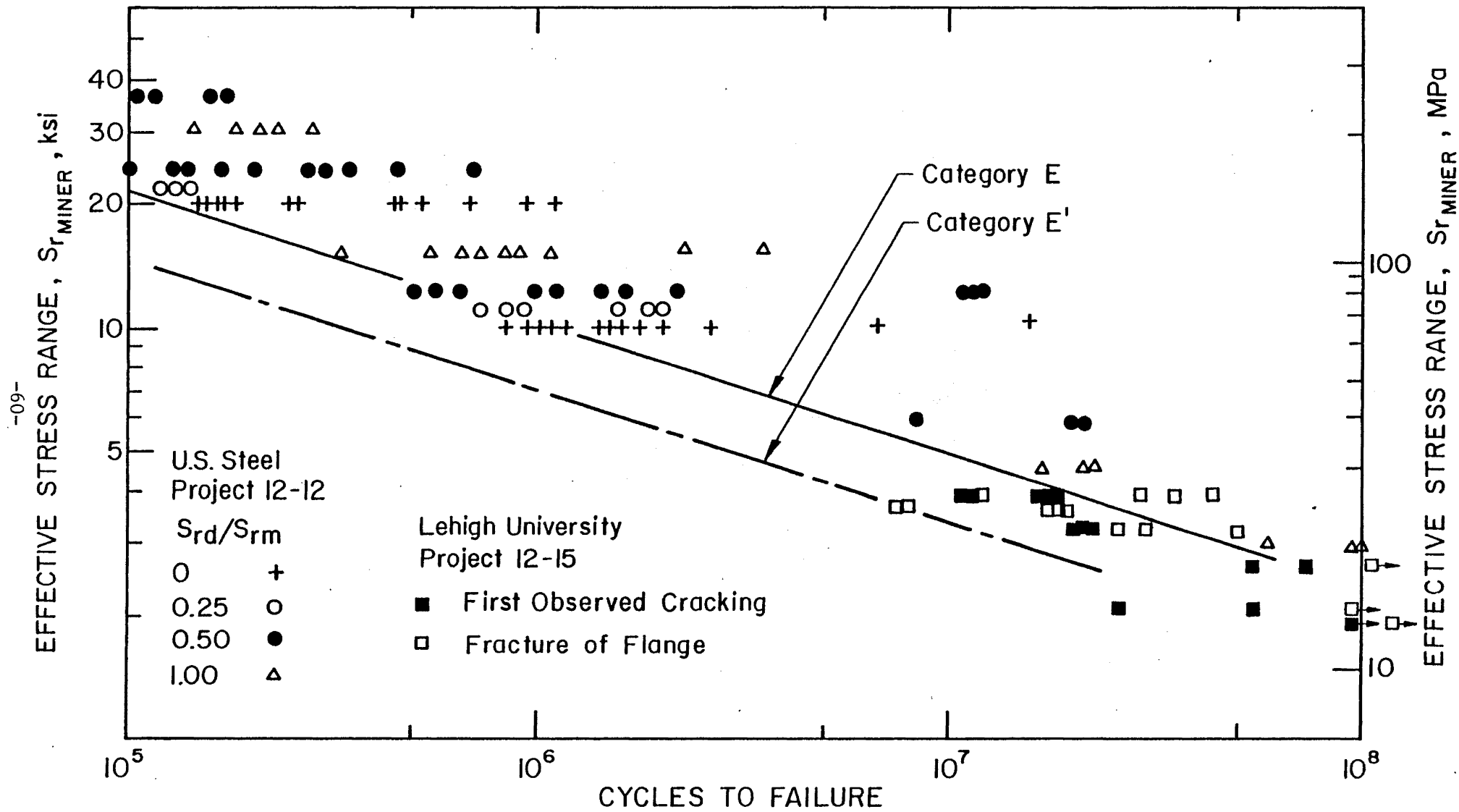


Fig. 24 Cover Plate Experimental Data

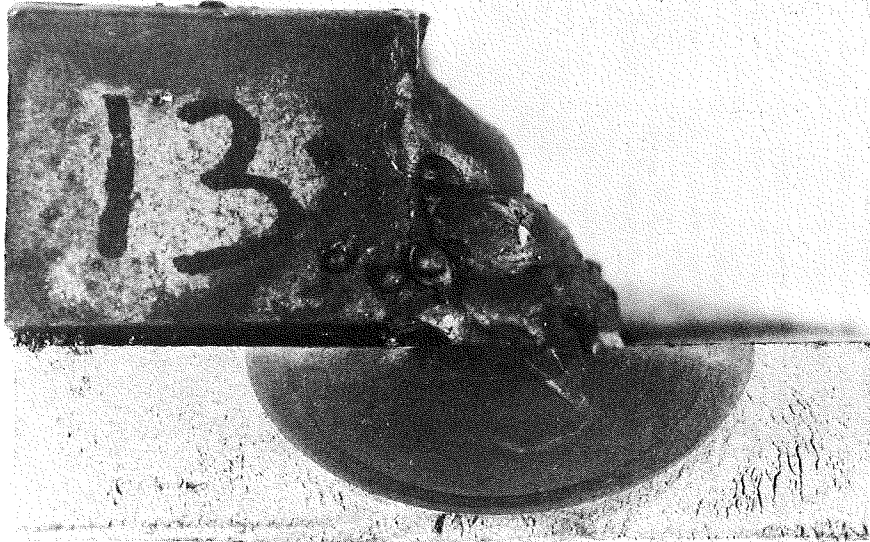


Fig. 25 Typical Fatigue Crack at
Longitudinal Weld Termination
(Beam A1 - East Cover Plate)

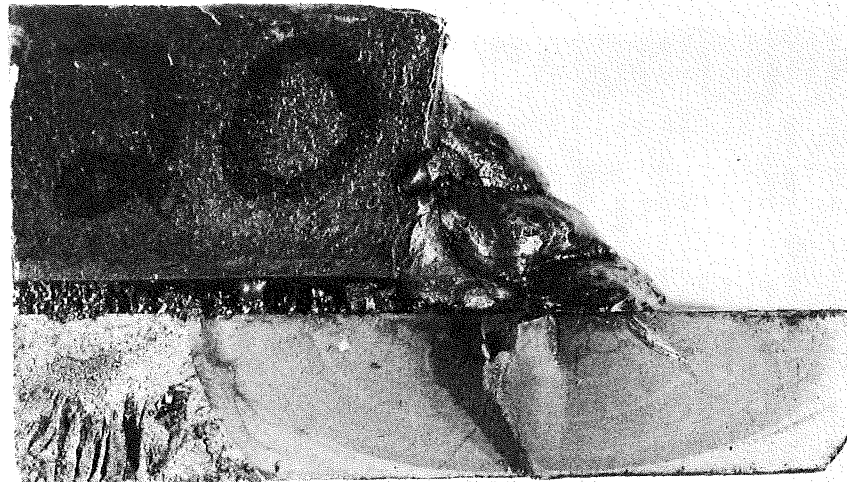


Fig. 26 Typical Through Crack at Weld Termination
(Beam C2 - West Cover Plate)

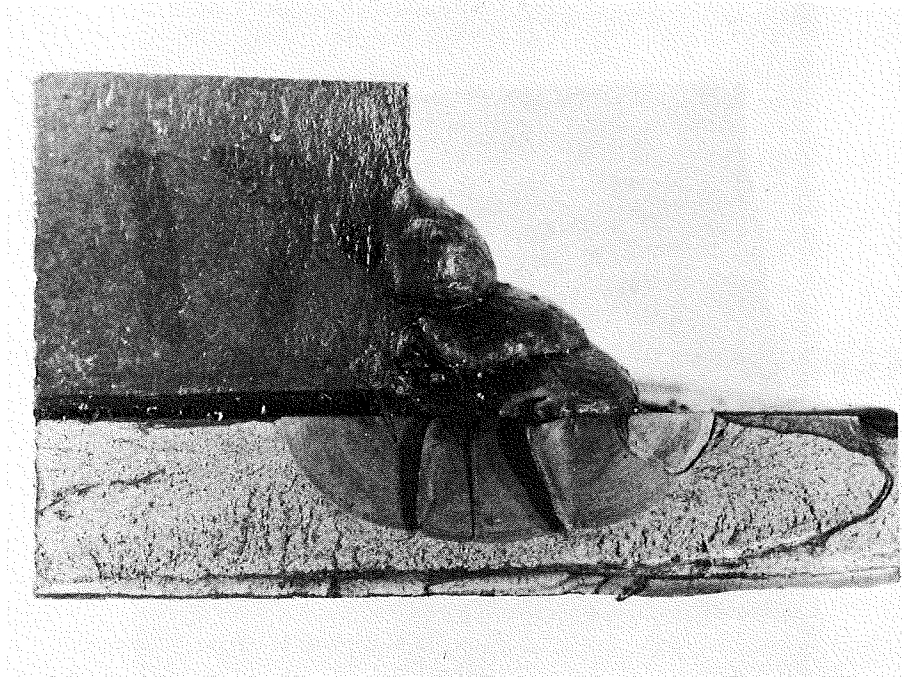


Fig. 27 Cracking Along Different Planes
at Weld Termination
(Beam A2 - West Cover Plate)

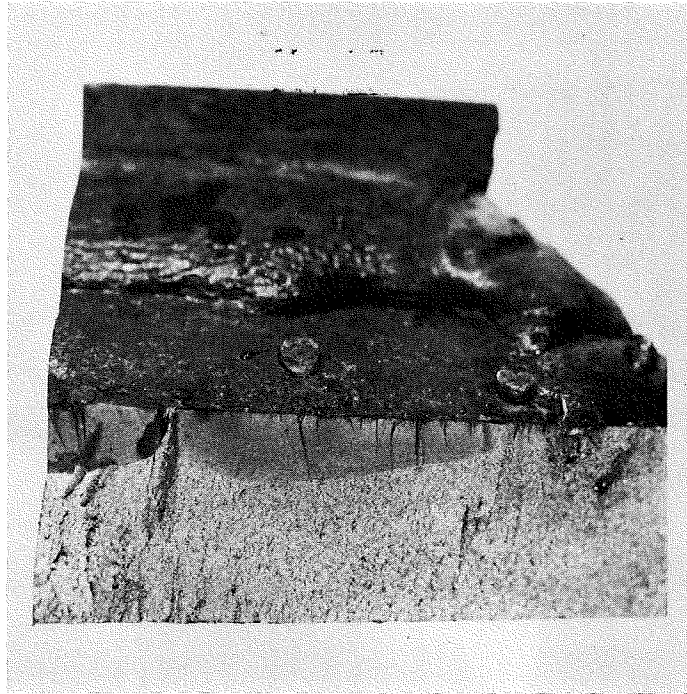


Fig. 28 Typical Fatigue Cracks Along
Transverse Weld Toe
(Beam A1 - East Cover Plate)



Fig. 29 Individual Cracks Before Coalescing
into One Long Edge Crack
(Beam A1 - West Cover Plate)

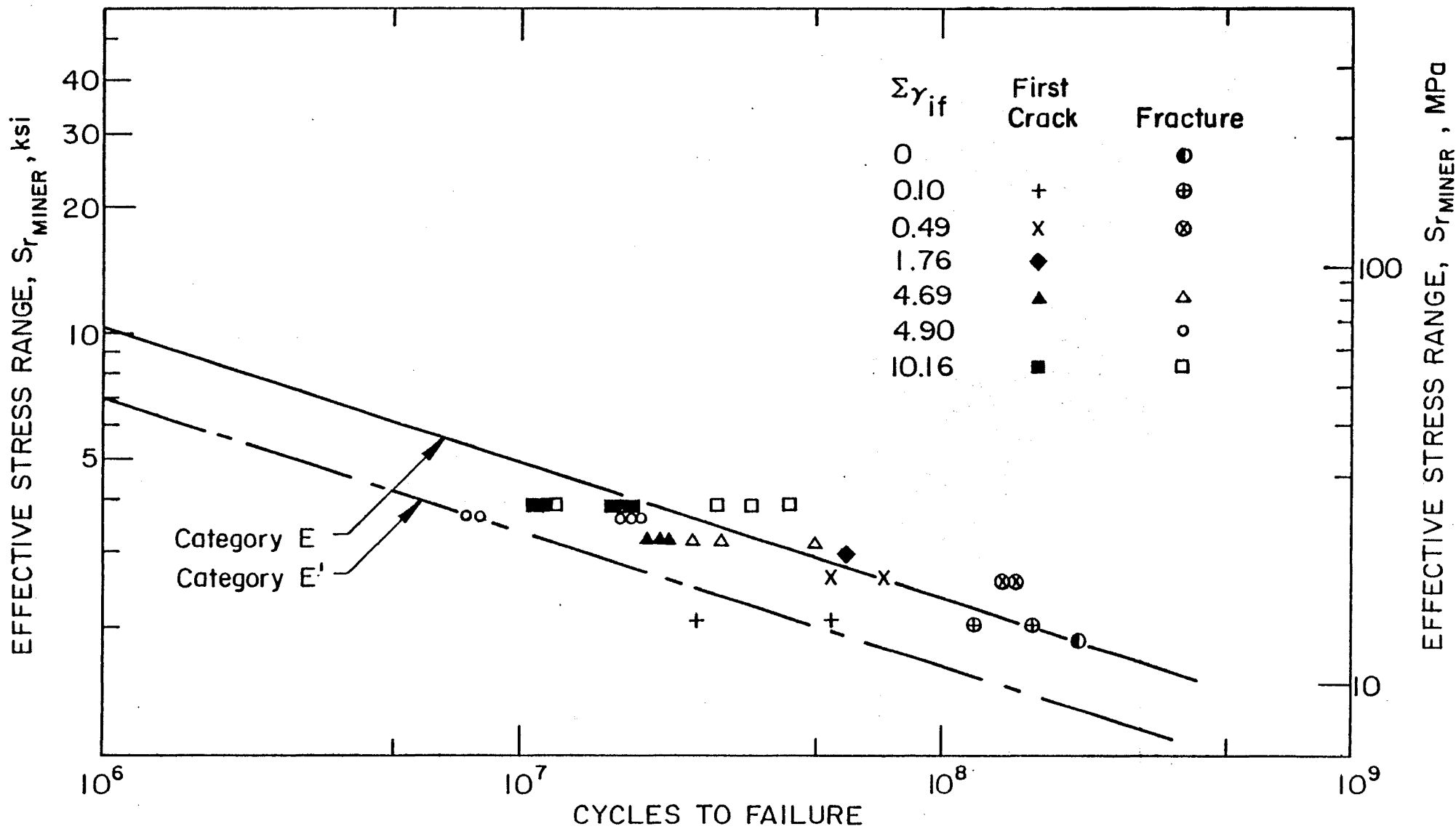


Fig. 30 Cover Plate Experimental Data



Fig. 31 Crack Development Along Transverse Weld Toe
After 100 Million Cycles
(Beam B1 - East Cover Plate)

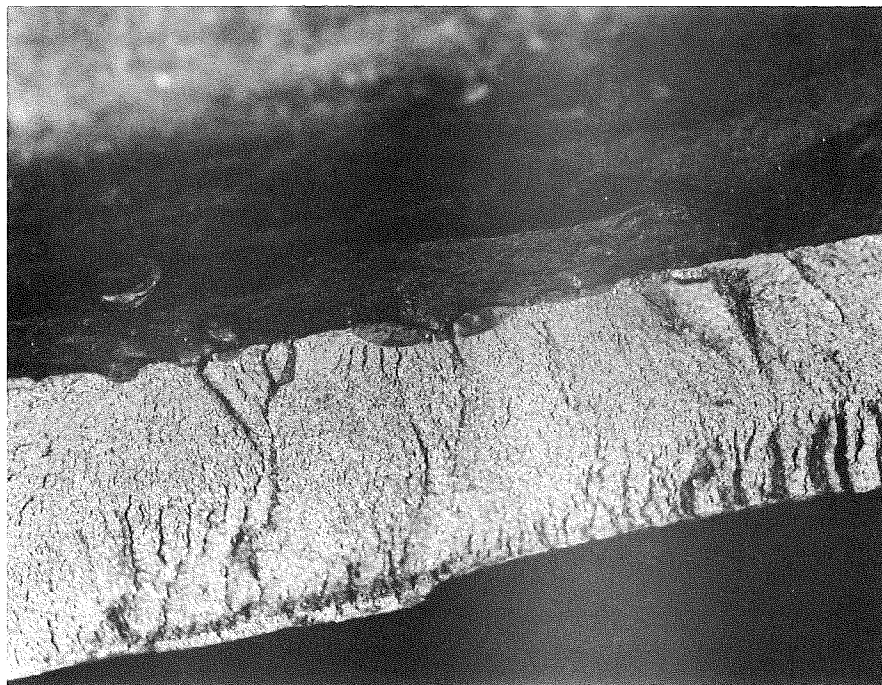


Fig. 32 Crack Development Along Transverse Weld Toe
After 100 Milliom Cycles
(Beam B1 - West Cover Plate)

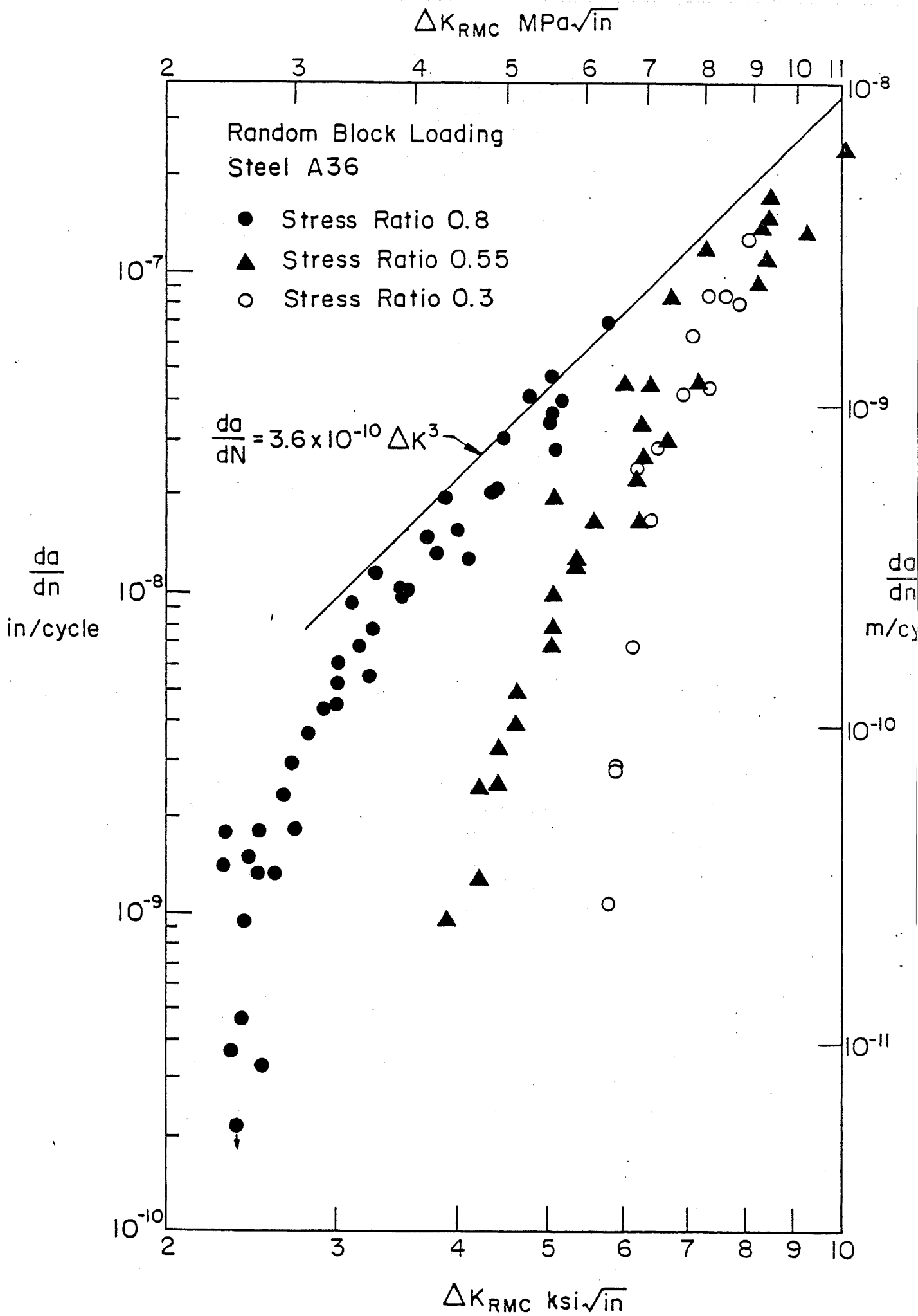


Fig. 33 Fatigue Crack Growth Test Data

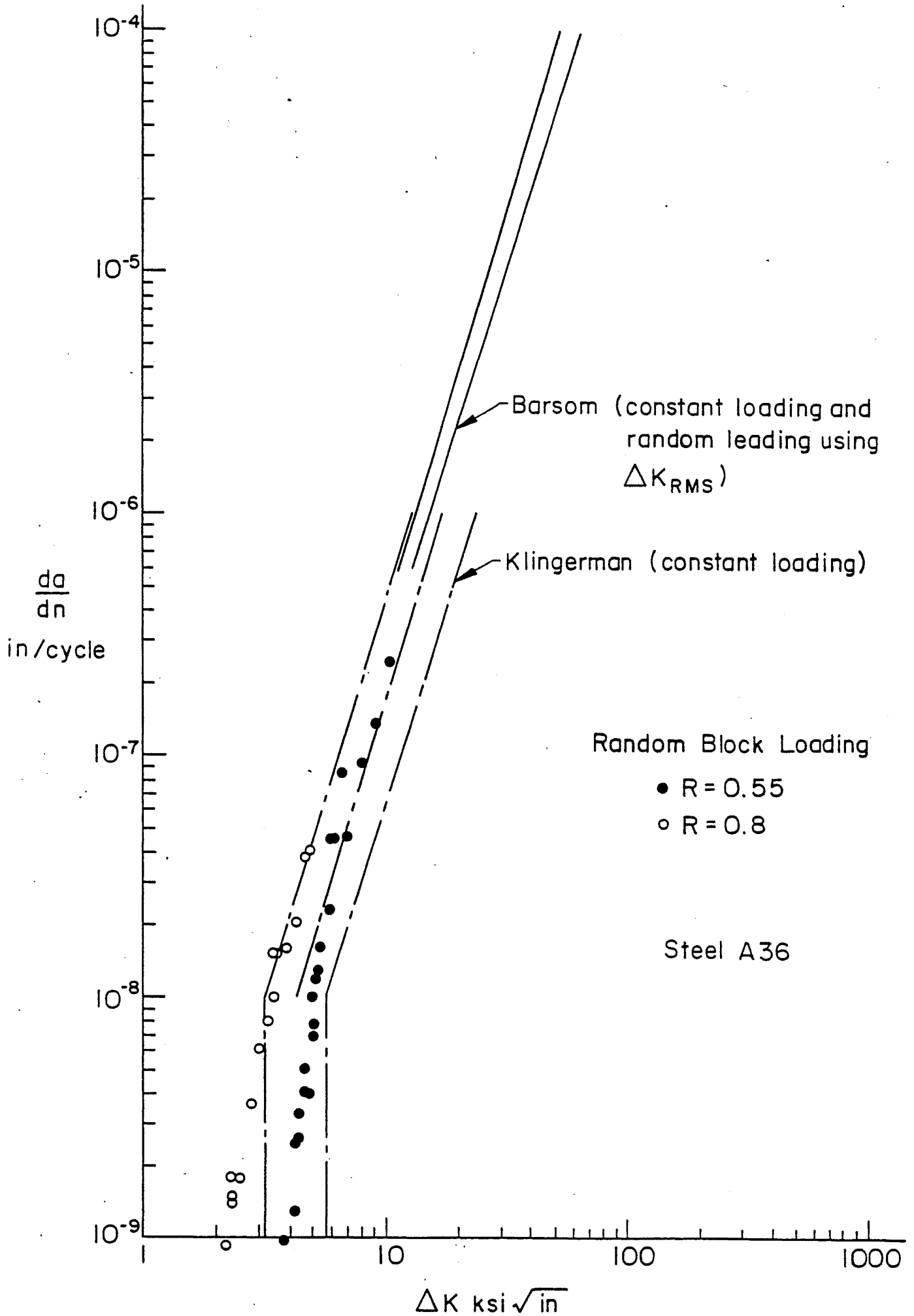


Fig. 34 Test Data Compared with Scatter Bands Observed by Klingerman and Barsom

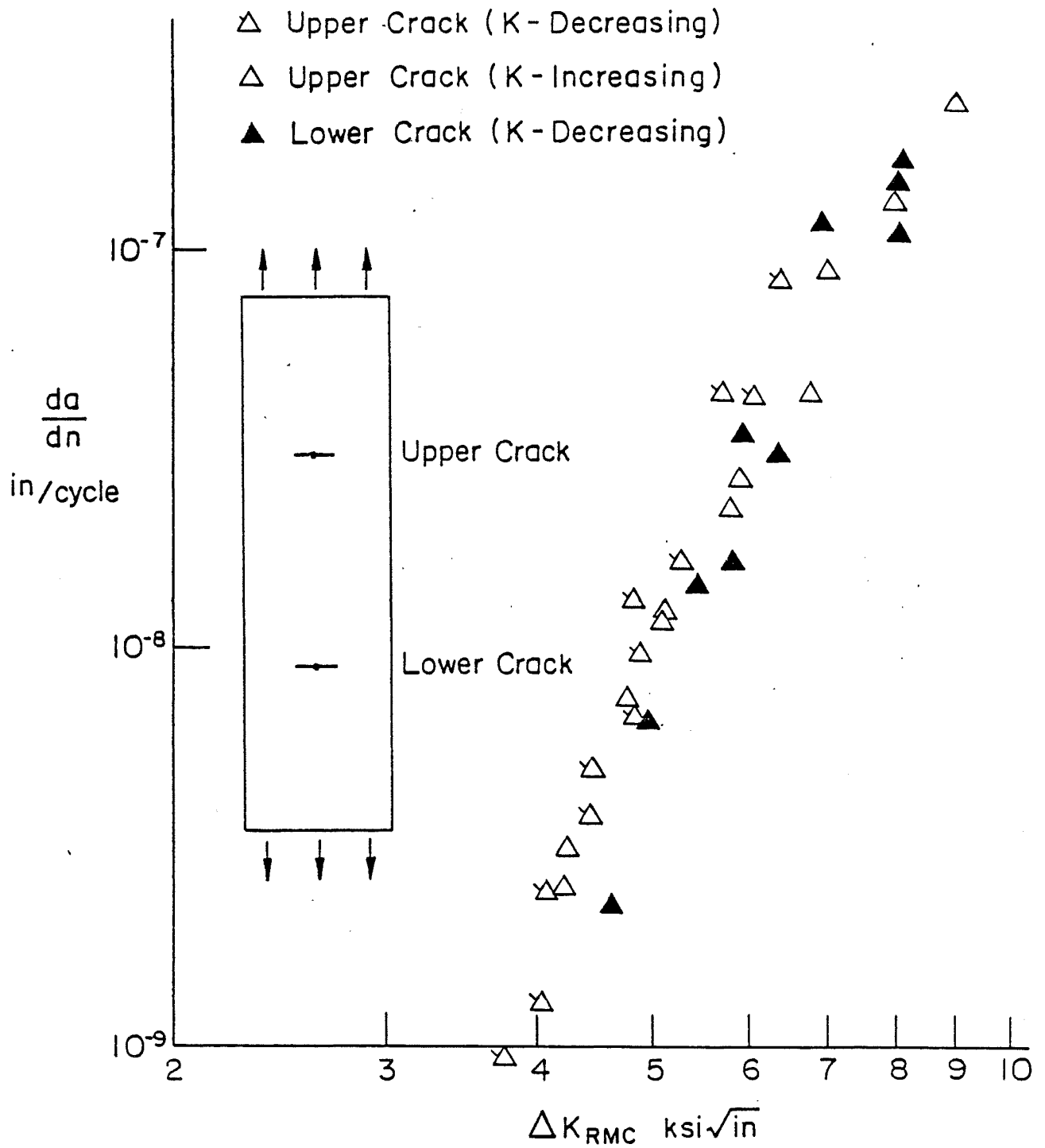


Fig. 35 Data Acquired from ΔK Decreasing and ΔK Increasing

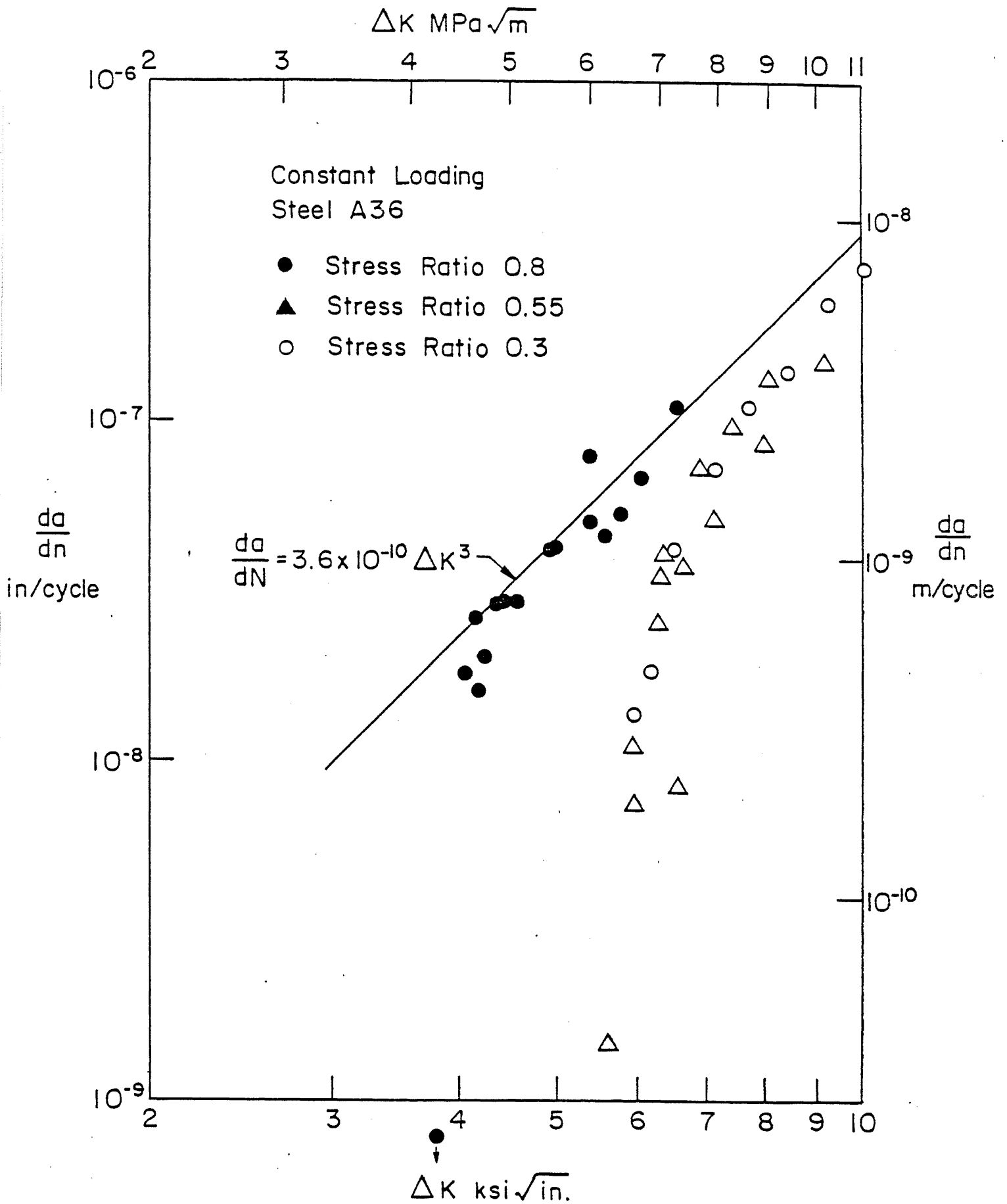
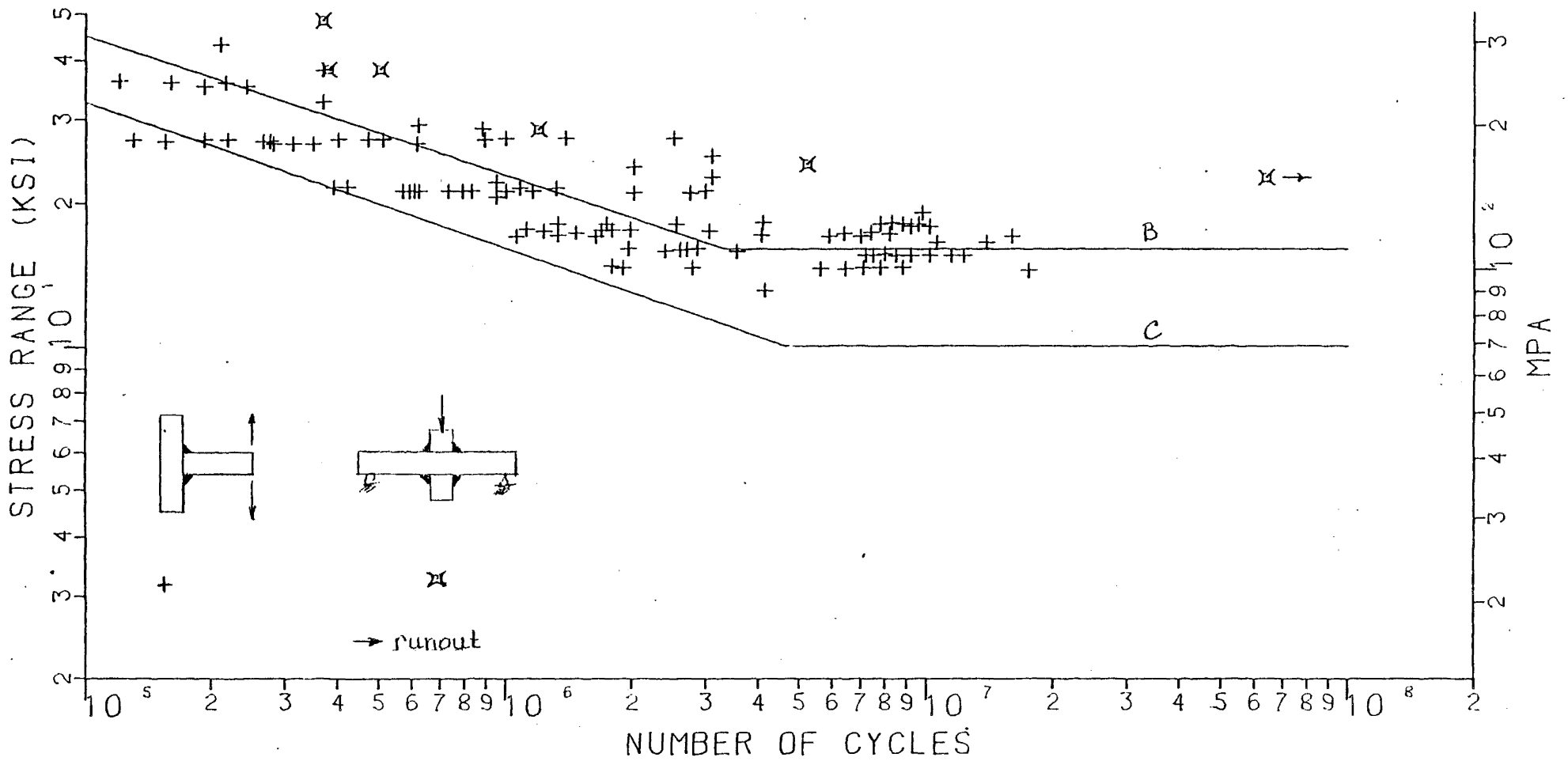


Fig. 36 Constant Amplitude Crack Growth Data



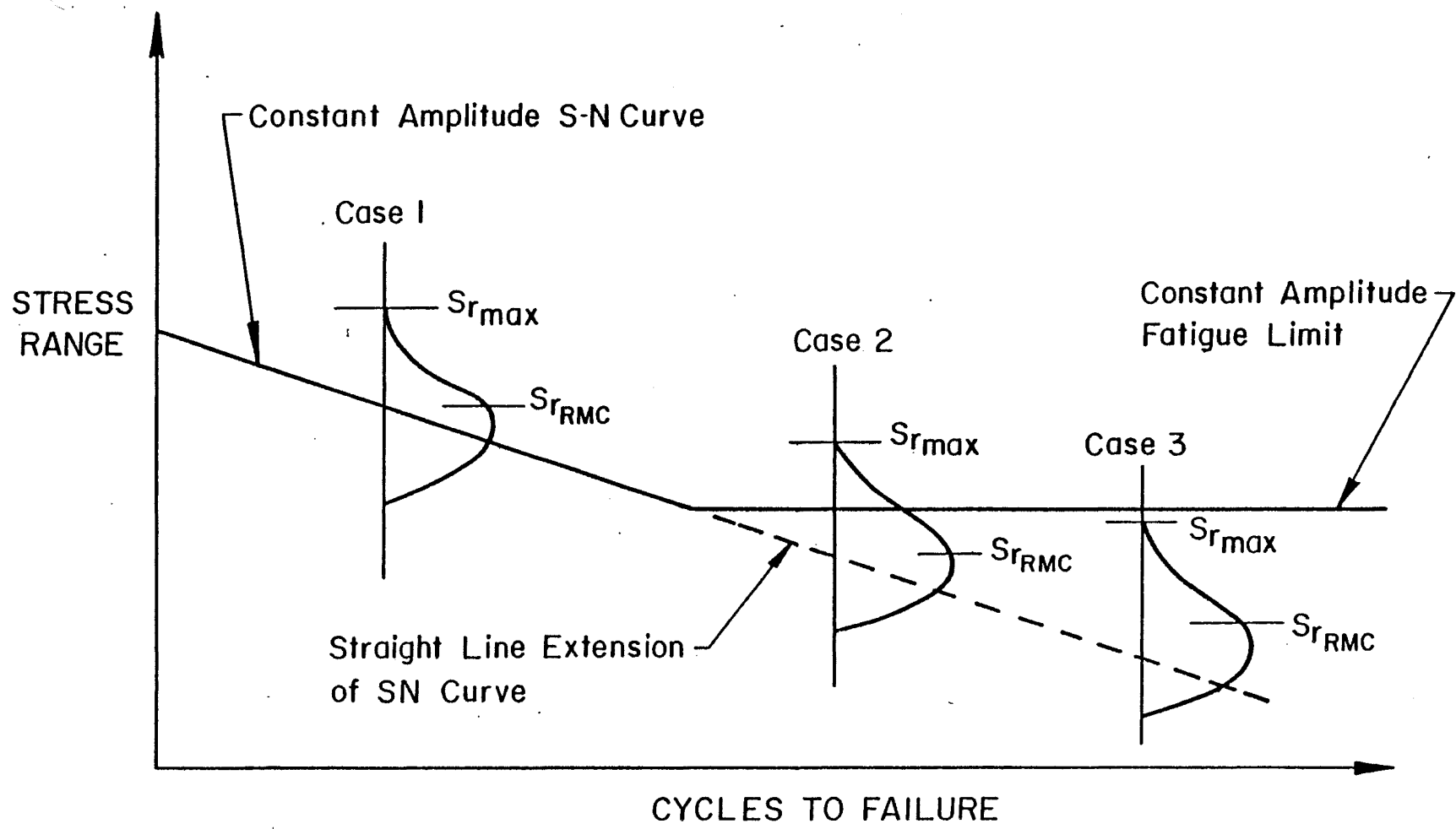


Fig. 39 Three Cases of Variable Amplitude Stress Spectra

TABLE A1: WEB ATTACHMENTS

<u>Beam No.</u>	<u>Detail</u>	<u>End</u>	<u>Cycles @ Retrofit (Through Crack) $a \approx 25 \text{ mm (1.0 in.)}$</u>	<u>Cycles @ Completion of Test</u>
A1	West	West	22.9×10^6	} 26.1×10^6
		East	----	
	Middle	West	17.8×10^6	
		East	----	
	East	West	17.8×10^6	
		East	15.5×10^6	
A2	West	West	----	} 26.1×10^6
		East	19.0×10^6	
	Middle	West	----	
		East	----	
	East	West	----	
		East	16.5×10^6	
B1	West	West	71.0×10^6	} 100.0×10^6
		East	----	
	Middle	West	----	
		East	----	
	East	West	----	
		East	70.0×10^6	
B2	West	West	40.5×10^6	} 60.0×10^6
		East	31.2×10^6	
	Middle	West	31.2×10^6	
		East	35.7×10^6	
	East	West	28.1×10^6	
		East	----	

TABLE A1: WEB ATTACHMENTS (continued)

<u>Beam No.</u>	<u>Detail</u>	<u>End</u>	<u>Cycles @ Retrofit (Through Crack) a ≈ 25 mm (1.0 in.)</u>	<u>Cycles @ Completion of Test</u>
C1	West	West	13.6 x 10 ⁶	} 17.1 x 10 ⁶
		East	11.9 x 10 ⁶	
	Middle	West	9.1 x 10 ⁶	
		East	----	
	East	West	13.0 x 10 ⁶	
		East	16.8 x 10 ⁶	
C2	West	West	16.1 x 10 ⁶	} 17.1 x 10 ⁶
		East	15.7 x 10 ⁶	
	Middle	West	13.0 x 10 ⁶	
		East	----	
	East	West	13.6 x 10 ⁶	
		East	10.7 x 10 ⁶	
D1	West	West	103.6 x 10 ⁶	} 150 x 10 ⁶
		East	116.2 x 10 ⁶	
	Middle	West	112.2 x 10 ⁶	
		East	112.2 x 10 ⁶	
	East	West	127.0 x 10 ⁶	
		East	103.6 x 10 ⁶	
D2	West	West	110.0 x 10 ⁶	} 120.0 x 10 ⁶
		East	110.0 x 10 ⁶	
	Middle	West	110.0 x 10 ⁶	
		East	110.0 x 10 ⁶	
	East	West	110.0 x 10 ⁶	
		East	110.0 x 10 ⁶	

TABLE A2: COVER PLATE DETAILS

<u>Beam No.</u>	<u>Detail</u>	<u>Cycles @ First Cracking</u>	<u>Cycles @ Failure</u>
A1	West	21.4×10^6	25.9×10^6
	East	21.4×10^6	30.6×10^6
A2	West	17.5×10^6	17.5×10^6
	East	19.5×10^6	19.5×10^6
B1	West	----	$200.0 \times 10^{6*}$
	East	----	$200.0 \times 10^{6*}$
(Cracks Found by Destructive Testing)			
B2	West	28.1×10^6	$120.0 \times 10^{6*}$
	East	60.0×10^6	$150.0 \times 10^{6*}$
C1	West	7.25×10^6	7.25×10^6
	East	7.25×10^6	7.25×10^6
C2	West	10.7×10^6	10.7×10^6
	East	----	$44.0 \times 10^{6*}$
(Cracks Found by Destructive Test)			
D1	West	80.0×10^6	150.0×10^6
	East	80.0×10^6	140.0×10^6
D2	West	60.0×10^6	130.0×10^6
	East	60.0×10^6	130.0×10^6

*Estimated life based on size of crack found by destructive testing

TABLE A3

Specimen No. 1 - Upper Crack
 Width of Specimen = 3.5 B = .25
 Stress Ratio = .55
 AN = .19
 $S_{rd}/S_{rm} = .5 \quad (S_{rmax} - S_{rmin})/S_{rd} = 3$

<u>No.</u>	<u>A(in.)</u>	<u>N(Cycles)</u>	<u>S_{rRMC}</u>
1	.4075	0	
2	.4575	582000	5.55
3	.493	1.37500E+06	5.00
4	.5325	2.24800E+06	4.50
5	.53875	2.61600E+06	4.05
6	.5425	2.80000E+06	3.64
7	.55125	3.44700E+06	3.64
8	.5555	4.06500E+06	3.64
9	.565	5.01300E+06	3.64
10	.57	6.29600E+06	3.28
11	.576	7.48600E+06	3.28
12	.5785	9.42400E+06	2.95
13	.59525	1.61620E+07	2.95
14	.6125	3.35240E+07	2.65
15	.62	3.64310E+07	2.95
16	.63075	3.97190E+07	2.95
17	.6345	4.06290E+07	3.28
18	.6405	4.13980E+07	3.28
19	.652	4.23480E+07	3.43
20	.65875	4.28720E+07	3.43
21	.67325	4.34950E+07	3.89
22	.68725	4.40070E+07	3.89
23	.70575	4.44110E+07	4.36
24	.7085	4.44740E+07	4.36
25	.7425	4.46260E+07	7.35
26	.78075	4.50360E+07	4.72
27	.82575	4.53670E+07	5.28
28	.85825	4.55000E+07	5.60

Note: 1 inch = 25.4 mm
 1 ksi = 6.895 Mpa

TABLE A4

Specimen No. 2 - Lower Crack
 Width of Specimen = 3.5 B = .25
 Stress Ratio = .8
 AN = .19
 $S_{rd}/S_{rm} = .5$ $(S_{rmax} - S_{RMIN})/S_{rd} = 3$

<u>No.</u>	<u>A(in.)</u>	<u>N(Cycles)</u>	<u>S_{rRMC}</u>
1	.2775	0	
2	.30675	685000	4.85
3	.3305	1.44900E+06	4.32
4	.3415	2.27300E+06	3.92
5	.36	3.63600E+06	3.53
6	.3805	5.56800E+06	3.18
7	.3875	6.80600E+06	2.86
8	.401	7.94400E+06	2.86
9	.41625	1.00100E+07	2.58
10	.41625	1.31340E+07	2.32
11	.425	1.89050E+07	2.09
12	.4205	1.89050E+07	2.58
13	.435	2.04460E+07	2.58
14	.453	2.30520E+07	2.58
15	.469	2.66940E+07	2.32
16	.492	3.44880E+07	2.09
17	.5109	4.86500E+07	1.97
18	.5355	8.15690E+07	1.77
19	.56775	9.51410E+07	1.88
20	.58775	9.88950E+07	2.09
21	.603	1.00374E+08	2.32
22	.62	1.01244E+08	2.58
23	.641	1.02219E+08	2.86
24	.6535	1.02478E+08	3.18
25	.66075	1.02684E+08	3.18
26	.673	1.03113E+08	3.18
27	.695	1.03420E+08	3.53
28	.74	1.03679E+08	4.23
29	.741	1.04009E+08	4.36

Note: 1 inch = 25.4 mm
 1 ksi = 6.895 MPa

TABLE A5

Specimen No. 2 - Upper Crack
 Width of Specimen = 3.5 B = .25
 Stress Ratio = .8
 AN = .19
 $S_{rd}/S_{rm} = .5 \quad (S_{rmax} - S_{rmin})/S_{rd} = 3$

<u>No.</u>	<u>A(in.)</u>	<u>N(Cycles)</u>	<u>S_{rRMC}</u>
1	.3025	0	
2	.3305	685000	5.04
3	.35925	1.44900E+06	4.69
4	.3765	2.27300E+06	3.96
5	.398	3.63600E+06	3.53
6	.42675	5.56800E+06	3.18
7	.43925	6.80600E+06	2.86
8	.4575	7.94400E+06	2.86
9	.47375	1.00100E+07	2.58
10	.49325	1.31340E+07	2.32
11	.5145	1.89050E+07	2.09
12	.52425	2.42320E+07	1.88
13	.5245	2.59730E+07	1.69
14	.53925	3.41660E+07	1.69
15	.5555	4.50260E+07	1.73
16	.5555	9.82470E+07	1.68
17	.56	1.11647E+08	1.78
18	.567	1.26421E+08	1.69
19	.572	1.31711E+08	1.69
20	.582	1.58431E+08	1.62

Note: 1 inch = 25.4 mm
 1 ksi = 6.895 MPa

TABLE A6

Specimen No. 3 - Upper Crack

Width of Specimen = 3.5 B = .25

Stress Ratio = .3

AN = .19

$S_{rd}/S_{rm} = .5$ $(S_{rmax} - S_{rmin})/S_{rd} = 3$

<u>No.</u>	<u>A(in.)</u>	<u>N(Cycles)</u>	<u>S_{RMC}</u>
1	.2535	0	
2	.271	20300	8.21
3	.29	433000	8.21
4	.3055	777000	7.39
5	.319	1.31100E+06	6.04
6	.339	4.17200E+06	5.80
7	.345	1.33330E+07	5.38
8	.3595	1.70050E+07	5.38
9	.3685	2.81930E+07	4.77
10	.3695	7.12860E+07	4.36
11	.371	8.73230E+07	4.78
12	.464	9.05350E+07	5.38
13	.502	9.11190E+07	5.38
14	.5215	9.12650E+07	5.98
15	.5455	9.15590E+07	5.26
16	.569	9.20770E+07	4.85
17	.594	9.35460E+07	4.36
18	.599	9.53380E+07	3.92

Note: 1 inch = 25.4 mm
1 ksi = 6.895 MPa

TABLE A7

NONLOAD-CARRYING WELDS UNDER VARIABLE AMPLITUDE

<u>S_{rmin}</u> (ksi)	<u>S_{rmax}</u> (ksi)	<u>S_{mean}</u> (ksi)	<u>S_{rRMC}</u> (ksi)	<u>N</u>
7.48	28.46	31.61	17.67	100,000,000 ⁺
11.88	38.12	31.02	23.67	7,025,000
12.18	38.12	31.37*	23.67	100,000,000 ⁺
15.42	48.31	30.95	30.0	1,251,000
15.51	48.31	31.96	30.0	991,000
12.27	41.50	32.21	25.79	677,000
12.19	38.12	30.73	23.67	4,408,000
9.20	31.30	30.90	19.33	1,637,000

TABLE A8

NONLOAD-CARRYING WELDS UNDER CONSTANT AMPLITUDE

<u>S_{mean}</u> (ksi)	<u>S_r</u> (ksi)	<u>N</u>
31.22	38.12	502,000
30.87	38.12	379,000
30.85	48.31	368,000
30.15	28.46	1,199,000
30 ⁺	22	62 - 63 x 10 ⁶

Note: 1 ksi = 6.895 MPa

*At 45,699,000 cycles the S_{mean} = 29.57 ksi for the duration of the test

⁺No apparent cracking

REFERENCES

1. Schilling, C. G., Klippstein, K. H., Barsom, J. M., and Blake, G. T. "Fatigue of Welded Steel Bridge Members under Variable-Amplitude Loadings," NCHRP Report 188 (1978), 113 pp.
2. Albrecht, P. and Friedland, A. M., "Fatigue-Limit Effect on Variable-Amplitude Fatigue of Stiffeners," J. Struct. Div., ASCE, Vol. 105, No. ST12 (Dec. 1979), pp. 2657-2675.
3. Fisher, J. W., Slockbower, R. E., Hausammann, H., and Pense, A. W., "Long Time Observation of a Fatigue Damaged Bridge," ASCE Proceedings, Vol. 107, No. TC1 (April 1981), pp. 55-71.
4. Tilly, G. P. and Nunn, D. E., "Variable Amplitude Fatigue in Relation to Highway Bridges," Proceedings, Institution of Mechanical Engineers, Vol. 194 (1981), p. 550.
5. Barsom, J. M. and Novak, S. R., "Subcritical Crack Growth in Steel Bridge Members," NCHRP Report 181 (1977), p. 82.
6. Bucci, R. J., "Fatigue Crack Growth Measurement and Data Analysis," ASTM STP 738, American Society for Testing and Materials (1981), p. 5.
7. "Proposed ASTM Test Method for Measurement of Fatigue Crack Growth Rates," ASTM STP 738, American Society for Testing and Materials (1981), p. 340.

8. Frank, K. H. and Fisher, J. W., "Fatigue Strength of Fillet Welded Cruciform Joints," ASCE Proceedings, Vol. 105, No. ST9 (Sept. 1979), pp. 1727-1740.
9. Fisher, J. W., Barthelemy, B. M., Mertz, D. R., and Edinger, J. A., "Fatigue Behavior of Full-Scale Welded Bridge Attachments," NCHRP 227 (1979) 47 pp.
10. Rolfe, S. T. and Barsom, J. M., "Fracture and Fatigue Control in Structures," Application of Fracture Mechanics, Prentice-Hall, Inc. (1977).
11. Klingerman, D. J., "Threshold Crack Growth in A36 Steel," M. S. Thesis, Lehigh University (1973).
12. Fisher, J. W., Albrecht, P. A., Yen, B. T., Klingerman, D. J., and McNamee, B. M., "Fatigue Strength of Steel Beams with Welded Stiffeners and Attachments," NCHRP Report 147 (1974), p. 85.
13. Fisher, J. W., Hausammann, H., Sullivan, M. D., and Pense, A. W., "Detection and Repair of Fatigue Damage in Welded Highway Bridges," NCHRP Report 206 (1979), p. 85.
14. Fisher, J. W., Frank, K. H., Hirt, M. A., and McNamee, B. M., "Effect of Weldments on the Fatigue Strength of Steel Beams," NCHRP Report 102 (1970), p. 114.
15. Berger, P., "Fatigue Testing of Welded Beams," Proceedings, IABSE Colloquium Lausanne, Vol. 37 (1982), pp. 323-330.

16. Yamada, K. and Kikuchi, Y., "Fatigue Behavior of 2- and 4-Year Weathered Welded Joints," Nagoya University, August 1983.
17. "Fatigue Phenomena in Welded Connections of Bridges and Cranes," Question D 130, Report No. 10, Office of Research and Experiments of the International Union of Railways (1979), p. 35.
18. Albrecht, P., "Fatigue Behavior of Weathered Steel Bridge Components," FHWA/MD-81/02, University of Maryland (1982).
19. Fisher, J. W., "Bridge Fatigue Guide, Design and Details," American Institute of Steel Construction (1977).
20. Goerg, P., "Uber die Aussagefahigkeit von Dauerversuchen mit Prufkorpern aus Baustahl ST37 und ST52," Der Stahlbau, Vol. 32, No. 2, 1963.
21. Mueller, J. A. and Yen, B. T., "Girder Web Boundary Stresses and Fatigue," Welding Research Council Bulletin 127, 1968.